UNIVERSIDAD DE CHILE
FACULTAD DE CIENCIAS FÍSICAS Y MATEMÁTICAS
DEPARTAMENTO DE INGENIERÍA MECÁNICA

RELIABILITY-BASED SELECTION OF MANUFACTURING TOLERANCE OF JOURNAL BEARINGS BY MEANS OF ADAPTIVE KRIGING METAMODEL

TESIS PARA OPTAR AL GRADO DE
MAGÍSTER EN CIENCIAS DE LA INGENIERÍA, MENCIÓN MECÁNICA

MEMORIA PARA OPTAR AL TÍTULO DE
INGENIERO CIVIL MECÁNICO

DIEGO ANDRÉS HIDALGO SILVA

PROFESOR GUÍA:
RAFAEL RUIZ GARCÍA

MIEMBROS DE LA COMISIÓN:
VIVIANA MERUANE NARANJO
ADOLFO DELGADO MÁRQUEZ

Este trabajo ha sido parcialmente financiado por
ANID/FONDECYT/11180812 - ANID-PFCHA/MagísterNacional/2019-22191415

SANTIAGO DE CHILE
2021

RESUMEN DE LA MEMORIA PARA OPTAR
AL TÍTULO DE MAGISTER EN CIENCIAS
DE LA INGENIERÍA, MENCIÓN MECÁNICA
POR: DIEGO ANDRÉS HIDALGO SILVA
FECHA: 2021
PROF. GUÍA: RAFAEL RUIZ GARCÍA

RELIABILITY-BASED SELECTION OF MANUFACTURING TOLERANCE OF JOURNAL BEARINGS BY MEANS OF ADAPTIVE KRIGING METAMODEL

Uncertainties are present in any engineering system, from the modeling and design up to the manufacturing and performance. The performance of a system based on nominal design parameters may significantly differ from that of the final product. These discrepancias are related to uncertainties associated with the manufacturing process and material properties, which have been traditionally mitigated with strict tolerance specifications and process control parameters, respectively.

Traditionally, tolerancing specification is based on pure geometrical analysis trying to minimize undesired effects in the component assembly. However, the objective of this work is to identify the relationship between the manufacturing tolerance of a component and the expected variations on its mechanical performance. To the best of the authors' knowledge, such relationship has not been fully addressed in the literature.

A framework is proposed where the manufacturing tolerance is described through probability density functions while its effect on performance is addressed via stochastic simulations. The procedure underlies the adoption of a surrogate model under local and global training (based on adaptive Kriging interpolation) to predict the probability to exceed a certain performance. The proposed framework is illustrated and validated studying a tilting pad journal bearing in terms of minimum and maximum credible values for its dynamic coefficients. Results show a significant saving in terms of computational time, making this framework attractive to perform manufacturing tolerances selection.

RESUMEN DE LA MEMORIA PARA OPTAR
AL TÍTULO DE MAGISTER EN CIENCIAS
DE LA INGENIERÍA, MENCIÓN MECÁNICA
POR: DIEGO ANDRÉS HIDALGO SILVA
FECHA: 2021
PROF. GUÍA: RAFAEL RUIZ GARCÍA

DESARROLLO DE METAMODELOS ADAPTATIVOS BASADOS EN KRIGING PARA SELECCIÓN DE TOLERANCIAS DE FABRICACIÓN EN COJINETES HIDRODINÁMICOS

Las incertidumbres están presentes en cualquier sistema de ingeniería, desde el modelado y el diseño hasta la fabricación y su rendimiento. El rendimiento de un sistema basado en parámetros de diseño nominales puede diferir significativamente del producto final. Estas discrepancias están relacionadas con las incertidumbres asociadas al proceso de fabricación y las propiedades del material, las cuales tradicionalmente han sido mitigadas con estrictas especificaciones de tolerancia y parámetros de control del proceso, respectivamente

Tradicionalmente, la especificación de tolerancia se basa en un análisis geométrico puro que intenta minimizar los efectos no deseados en el ensamblaje del componente. Sin embargo, el objetivo de este trabajo es identificar la relación entre la tolerancia de fabricación de un componente y las variaciones esperadas en su rendimiento mecánico. Hasta donde saben los autores, dicha relación no se ha abordado plenamente en la bibliografía.

Se propone un marco en el que la tolerancia de fabricación se describe mediante funciones de densidad de probabilidad, mientras que su efecto sobre el rendimiento se aborda mediante simulaciones estocásticas. El procedimiento subyace a la adopción de un modelo sustituto bajo entrenamiento local y global (basado en la interpolación adaptativa de Kriging) para predecir la probabilidad de exceder un cierto rendimiento. El marco propuesto está ilustrado y validado estudiando un cojinete hidrodinámico en términos de valores mínimos y máximos creíbles para sus coeficientes dinámicos. Los resultados muestran un ahorro significativo en términos de tiempo computacional, lo que hace que este marco sea atractivo para realizar la selección de tolerancias de fabricación.

A mi familia y amigos
que siempre han estado presente.

Acknowledgment

En primer lugar, agradecer a mi familia, mis padres Cristina y Carlos y a mis hermanos Felipe y Vicente, quienes son mi pilar fundamental, gracias a ellos soy lo que soy hoy en día. Gracias por los valores que me inculcaron, por todas sus enseñanzas y su apoyo incondicional, me han respaldado en todas las etapas de mi vida y en todas mis decisiones. Mención también al Roco, por haber llegado a mi vida entregando siempre amor sincero.

También agradecer a todos mis amigos que siempre estuvieron presente y me alegran los días. Los del colegio, Juan Pablo, Nicolás, Luciano, Ignacio, Felipe C, Alejandro, Francisco, Felipe A, Iván y Julio, quienes hasta el día de hoy nos seguimos juntando conservando esta linda amistad. Mis amigos del plan común, Daniela, Danilo, Camilo, Ignacio, Margarita, Felipe R, Bastian, Marco y Francisco que me viene acompañando desde el primer día. Los de mecánica, José Tomás, Gabriel, Francisco C, Carlos, los del magister Alejandro y Bruno, haciendo de la universidad un espacio de amigos en el que disfrutaba pasar el día, agradezco mucho haberlos conocido y compartir tanto con ustedes.

Por otra parte, agradecer a mi segunda familia, familia Weis Palma que sé que puedo contar con ellos siempre, Lisette y Christian quienes son parte importante en mi vida, mis primos con los que las risas nunca faltan, mis cuñadas Lupita y Alexandra que las veo como mis hermanas y a mi polola Paula por todo el cariño y apoyo que me da contagiándome siempre con su alegría, gracias por todas esas risas y lindos momentos juntos.

Además, agradecer a la comisión de esta tesis y de forma muy especial deseo expresar mi agradecimiento al profesor Rafael Ruiz, quien durante estos últimos años ha sido muy importante en mi desarrollo profesional y personal, al entregarme siempre la confianza necesaria para extender mis conocimientos y avanzar en mi carrera profesional concretando metas y desarrollando nuevos proyectos.

Finalmente, agradecer el apoyo de la Agencia Nacional de Investigación y Desarrollo de Chile (ANID) a través del proyecto ANID/FONDECYT/11180812 y la beca de estudios de postgrado ANID-PFCHA/MagisterNacional/2019-22191415. Además, agradecer el apoyo y colaboración de la Universidad Texas A&M (TAMU) a través del Prof. Adolfo Delgado que hizo posible parte del trabajo plasmado en esta tesis y en un paper que se encuentra en revisión.

Contents

List of Tables

List of Figures

Chapter 1

Introduction

1.1 General Background

Uncertainties are present in any engineering system, from the modeling and design up to the manufacturing and performance. The performance of a system based on nominal design parameters may significantly differ from that of the final product. These discrepancies are related to uncertainties associated with the manufacturing process and material properties, which have been traditionally mitigated with strict tolerance specifications and process control parameters, respectively.

As performance limits are extended, acceptable deviation margins between nominal and actual performance lead to unrealistic machining tolerances, poor process control and quality targets. The only feasible approach is to embed all of the expected uncertainties within the design process. These uncertainties include (but are not limited to): (1) Design process: uncertain nature of excitations, lack of information about the model parameters, precision of the mathematical model; (2) Manufacturing: manufacturing process precision; and (3) Service and operation: deviation of product use from expected duty cycle.

The present work focuses on the study of manufacturing tolerances as part of the design process to predict system performance. The modern method of specifying tolerances is through geometric dimensioning and tolerancing (GD&T), as specified in the ASME Y14.5M Standard [1] and/or ISO 1101 [2]. Thus, the GD&T during product development is the first step in geometric variations management where its aim is to guarantee a specific performance by establishing permission limits of the geometric variations of a product due to its manufacturing process.

Traditionally, tolerancing specification is based on pure geometrical analysis trying to minimize undesired effects in the component assembly. It is possible to make a tolerance analysis and variation simulation from three main perspectives: (1) tolerance models representing the geometrical deviations on individual parts; (2) system behavioral models representing how variation propagates in a product or an assembly and (3) tolerance and variation analysis techniques [3].

Tolerance models represent the link between functional requirements and geometrical deviations of individual components in the form of mathematical expressions. There are different mathematical models for representing geometric deviation, such as variation geometry approach, skin model shape, and modal representation among others. Between these three classes, the most commonly used is the variation geometry approach, where the real geometry of parts is considered by the variation of nominal dimensions or it is bounded by a variation (position and orientation) of the nominal geometry [4]. The fundamentals of the skin model at a conceptual, geometric and computational level are investigated in [5], while the concept of skin model shapes that has been developed to address digital representation of "non-ideal" parts and extended to mechanical assemblies is studied in [6, 7, 8, 9]. Regarding modal representation, Huang et al. [10] propose a discrete-cosine-transformation (DCT) based on decomposition method for form defects modeling. Samper et al. [11] present the Discrete Modal Decomposition (DMD) considering modal shapes of a discretized feature. The geometric or dimensioning tolerances are represented by a deviation domain [12] or a Tolerance-Map® [13, 14, 15], while the orientation and position deviations of each surface could be represented by Technologically and Topologically Relates Surfaces (TTRS). These three models are compared in [16], and Chen et al. [17] provide a comprehensive review on dimensional tolerance analysis methods.

In order to analyze system behavior models, it is necessary to establish a relation between the allocated tolerances of the individual parts and the critical product dimension when creating the models. This kind of models can be divided into analytical and computer-aided models, the latter being the most promising strategy (for example, the work presented in [18, 19, 20]). Here, the tolerance analysis techniques can be applied adopting: (1) the worst-case analysis that considers the worst possible combinations of individual tolerances [21] or (2) statistical analysis that considers a probability density function of the manufacturing processes [22]. Both approaches compute the likelihood that the product can be assembled and will function under given individual tolerances. However, the objective of this work is not to determine if the final assembly will exclusively be possible under certain tolerances, but to establish the relationship between the manufacturing tolerance of specific components and the system-level performance associated with a specific mechanical functionality. To the best of the authors' knowledge, such relationship has not been fully addressed in the literature.

There are some mechanical components with functionalities that not only depend on the individual tolerances and their compatibility with the final assembly, but also in their ability to attain a specific performance. In these cases, it is crucial to perform a tolerance selection to evaluate its effect in the physics of the problem by employing different numerical simulation models. In this regard, it is proposed a scheme based on the probabilistic description of a mechanical component geometry in terms of the manufacturing tolerance. All statistical quantities are obtained using stochastic simulations, specifically adopting a Monte Carlo simulation. Therefore, one of the most challenging tasks is to manage the computer burden due to the large number of simulations needed to obtain an adequate approximation by the Monte Carlo simulation. To alleviate this computational demand, a surrogate model based on Kriging interpolation is proposed. This surrogate model is trained with the high-fidelity model in an adaptive manner to improve the accuracy of the model with the minimum number of support points. Two strategies are proposed, a metamodel trained in a global and a local manner. In order to provide an illustrative example and validate this study, these

proposed adaptive schemes are applied to identify the effect of the manufacturing tolerance in the dynamic performance of a tilting pad journal bearing (TPJB). These bearings are widely used in land-based turbomachinery to enable high-speed operation while avoiding subsynchronous instabilities [23] . TPJB are variable geometry bearings comprising multiple pads assembled around a bearing shell. Dmochowski et al. [24] and Quintini et al. [25] have reported that small variations in the pad clearance and preload (two well-known geometric parameters of TPJBs) lead to an important variation in the dynamic coefficients. This example illustrates the capability of the proposed framework to characterize the variation on mechanical performance as a function of the manufacturing tolerances not only for bearings but for any other mechanical component. However, it is considered particularly relevant for journal bearing applications since it could be easily implemented over new bearing configurations (for example [26, 27]) and the novel techniques developed to obtain their dynamic coefficients (for example [28, 29, 30]).

1.2 Objectives

The purpose of this work is to achieve the objectives presented below.

1.2.1 General Objective

Develop and implement a methodology that helps to identify the relationship between the manufacturing tolerance of a mechanical part and the expected variations on its mechanical performance.

1.2.2 Specific Objectives

- Propose and define a probabilistic framework that relates the manufacturing tolerances to the mechanical performance of different components.
- Propose a computational methodology based on the generation of metamodels in order to reduce the computational cost associated with the problem of propagation of uncertainties.
- Validate the methodology with an illustrative example.

1.3 Scope

- Implement the procedure in order to evaluate the effect of manufacturing tolerance on the dynamic performance of a tilting pad journal bearing (TPJB)

Chapter 2

General Overview of the Proposed Manufacturing Tolerance Selection Scheme

In order to support the proposal and analysis of this work, the next revision of the relevant concepts is carried out.

2.1 Manufacturing Tolerance Selection: Stochastic System Model and Performance Evaluation

The proposed framework is based on the probabilistic description of the geometry of a mechanical component as a function of the manufacturing tolerance. Hence, its performance could be also be expressed in probabilistic terms such that the manufacturing tolerance could be selected by employing a risk-related metric. For example, this approach could be used to select a manufacturing tolerance that yields a low probability of exceeding an admissible performance limit.

In order to establish the framework, it is necessary to describe the performance of the mechanical component of interest as $\mathbf{H}(\boldsymbol{\theta})$, where $\mathbf{H} \in \mathbb{R}^{n_H}$ corresponds to a deterministic performance metric, while $\boldsymbol{\theta} \in \mathbb{R}^{n_\theta}$ corresponds to all of parameters required in the performance assessment. In the context of this work, $\boldsymbol{\theta}$ is called the model parameters or model parameter vector. In engineering applications, model parameters are rarely known precisely due to the presence of uncertainties arising either from the mechanical properties (i.e. material imperfections) or from the geometry (i.e. variations introduced in the manufacturing process). These uncertainties are modeled adopting a Probability Density Function (PDF) $p(\boldsymbol{\theta})$ and propagated to the performance metric such that its expected value could be defined by solving the following probabilistic integral:

$$E[\mathbf{H}] = \int \mathbf{H}(\boldsymbol{\theta}) p(\boldsymbol{\theta}) \mathrm{d}\boldsymbol{\theta} \tag{2.1}$$

where $E[\mathbf{H}]$ defines the expected value of $\mathbf{H}$ after propagating the uncertainties associated with $\boldsymbol{\theta}$. Similarly, it is also possible to define the probability of $\mathbf{H}$ exceeding an admissible threshold:

$$P_F = P(\mathbf{H} > \mathbf{H}_{thresh}) = \int I_F(\boldsymbol{\theta}) p(\boldsymbol{\theta}) \mathrm{d}\boldsymbol{\theta} \tag{2.2}$$

where P_F defines the probability of $\mathbf{H}$ being greater than a threshold $\mathbf{H}_{thresh}$, also known as probability of exceedance. In this case, $I_F(\boldsymbol{\theta})$ corresponds to the indicator function that assumes a value of zero or one depending on whether the performance metric is below or above the threshold.

$$\begin{aligned} I_F(\boldsymbol{\theta}) &= 1 \ \text{ if } \ \mathbf{H}(\boldsymbol{\theta}) \geq \mathbf{H}_{thresh} \\ I_F(\boldsymbol{\theta}) &= 0 \ \text{ if } \ \mathbf{H}(\boldsymbol{\theta}) < \mathbf{H}_{thresh} \end{aligned} \tag{2.3}$$

At this point, all of the model parameters $\boldsymbol{\theta}$ are considered to have an unknown variation. However, and for the sake of simplicity, from now on $\boldsymbol{\theta}$ will exclusively denote the model parameters that are directly affected by the manufacturing tolerance. The next step is to relate the manufacturing tolerance (denote from now on as δ) to the distribution of the geometrical model parameters $p(\boldsymbol{\theta})$. This relation could be established by adopting the covariance matrix of $\boldsymbol{\theta}$ as function of δ, which is denoted as $\boldsymbol{\Sigma}_{\boldsymbol{\theta}}$. On the other hand, the expected value of $\boldsymbol{\theta}$ is defined using the nominal geometrical characteristics $\hat{\boldsymbol{\theta}}$ to avoid any bias between nominal geometry and the mean value of $p(\boldsymbol{\theta})$. Once the expected value and the covariance of $\boldsymbol{\theta}$ are defined, the remaining task is to define its distribution. In order to illustrate this relation, two distributions for $\boldsymbol{\theta}$ are presented in Fig.2.1. Here, both distributions $p(\boldsymbol{\theta})$ are assumed to be Gaussian with mean $\hat{\boldsymbol{\theta}}$ but with different variances. In particular, for the case presented in fig.2.1a the variance is defined as $\boldsymbol{\Sigma}_{\boldsymbol{\theta}} = \delta^2$ while the case presented in 2.1b corresponds to $\boldsymbol{\Sigma}_{\boldsymbol{\theta}} = (\delta/3)^2$, indicating that exist a probability of 0.681 and 0.997 that the given geometric characteristic of the mechanical component lies within the tolerance defined by δ. Note that the later PDF practically enforces that any possible geometry resulting in the manufacturing process will lie within the tolerance, while the former PDF corresponds to a more adverse scenario since it contemplates geometries outside of the tolerance. Ultimately, the relation between $\boldsymbol{\Sigma}_{\boldsymbol{\theta}}$ and δ together with the selection of the distribution $p(\boldsymbol{\theta})$ will be determined by the nature of the manufacturing process and the availability of uncertainty parameters. However, based on the principle of maximum entropy, it is possible to assume that the most adverse scenario corresponds to an independent Gaussian $p(\boldsymbol{\theta})$ with mean $\hat{\boldsymbol{\theta}}$ and variance δ^2 for each model parameter [31].

Once the manufacturing tolerance δ is defined, it is possible to solve Eq.(2.2) in order to evaluate the probability of exceedance P_F for different performance metric thresholds $\mathbf{H}_{thresh}$ (a detailed description of the computational procedure is presented in Section 2.2). The typical behavior of these two parameters is shown in Fig.2.2. The figure also includes results for different δ, which illustrate the impact of δ over P_F and $\mathbf{H}_{thresh}$.

Ultimately, the designer could select the manufacturing tolerance δ by adopting a risk-

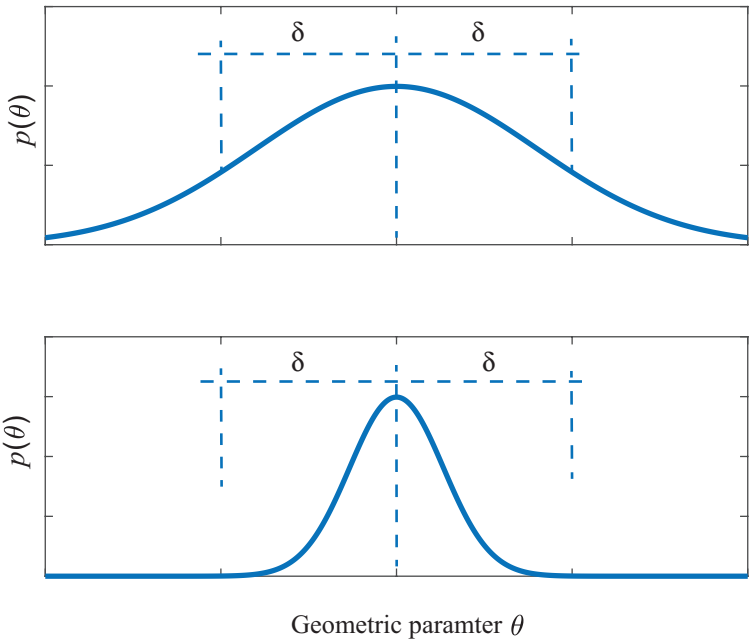

Figure 2.1: Relation between the manufacturing tolerance and the PDF associated to a geometrical parameter. Example for a single geometrical parameter defined by a Gaussian distribution

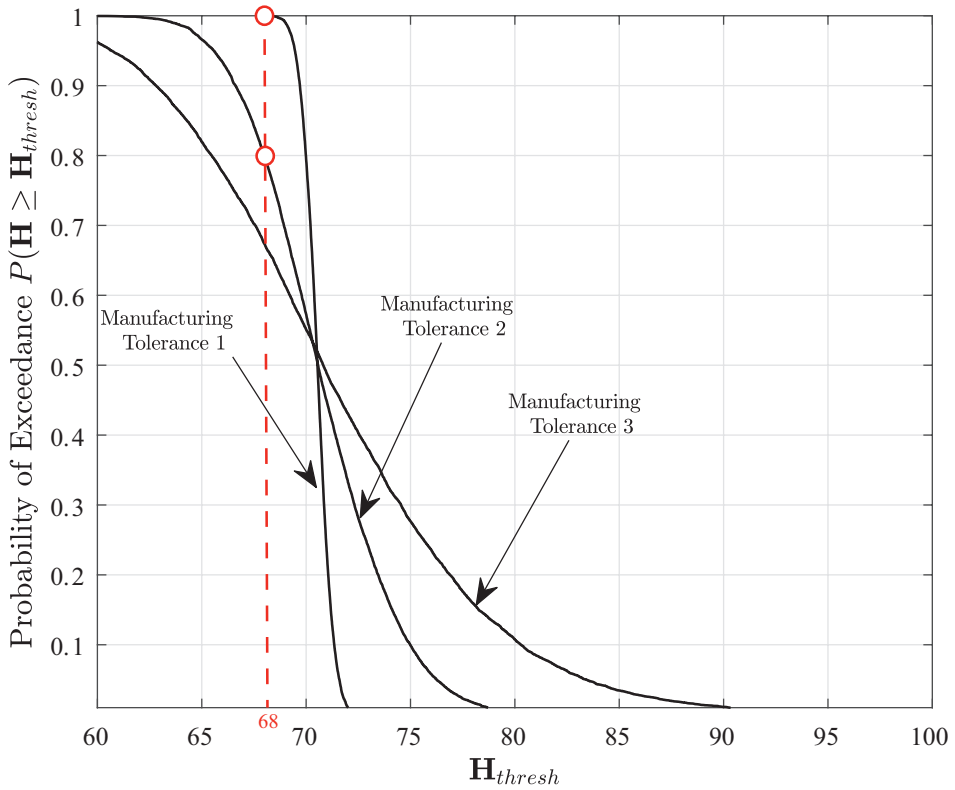

Figure 2.2: Example of probability of exceedance vs $\mathbf{H}_{thresh}$ for different manufacturing tolerance.

informed decision-making scheme. First, the threshold of the performance metric $\mathbf{H}_{thresh}$ is established, and then the manufacturing tolerance is selected based on a desired P_F. Note that the selection of P_F reveals the attitude towards risk of the designer, e.g., lower or higher P_F and P_F close to 0.5 indicate a risk-averse and a risk-neutral positions, respectively. To exemplify this, a reference line is included in Fig.2.2 (red dotted line) corresponding to $\mathbf{H}_{thresh} = 68$ (this number is chosen arbitrarily for the sake of the example). The selection of the third and second manufacturing tolerance lead to mechanical parts that have 100% and 80% probability to exhibit a performance greater than 68, respectively (see red circles in figure 2.2). This selection is considered a risk-averse attitude when the problem demands a performance higher that $\mathbf{H}_{thresh}$. On the other hand, if the problem demands a performance lower than $\mathbf{H}_{thresh}$, the risk-adverse attitudes lead to selection of lower exceedance probabilities. Furthermore, if the selection of the manufacturing tolerance is conducted based on a 50% of exceedance probability, it is said that the attitude towards risk is neutral since it exists 50% of chances to be above or below $\mathbf{H}_{thresh}$.

2.2 Stochastic Analysis and Computational Implementation

One of the most challenging task of the proposed framework relates to the recursive solution of the probabilistic integral presented in Eq.(2.2) for different manufacturing tolerances δ. The analytical calculation of this integral is impractical (apart from special, simple cases) and calculation through numerical integration is inefficient for $n_\theta > 3$. Therefore, a high-dimensional probabilistic integral is commonly solved via stochastic-simulations, corresponding to a broad class of computational methods that are sampling-based, e.g. Monte Carlo's Family Methods.

2.2.1 Stochastic Simulation Based on Monte Carlo Methods

The proposed methodology numerically approximates an integral of the form presented in Eq.(2.2). The first step of this method corresponds to the generation of K samples that follow $p(\boldsymbol{\theta})$ such that $\{\boldsymbol{\theta}^j, j = 1, ..., K\}$. The second step consists of estimating the output of the system by using each sample obtained previously, generating a set of data denoted $\{I_F(\boldsymbol{\theta}^j), j = 1, ..., K\}$. Finally, based on the Central Limit Theorem, the Monte Carlo method estimates the probabilistic integral (Eq. (2.2)) as:

$$\hat{P}_F \approx \frac{1}{K} \sum_{j=1}^{K} I_F(\boldsymbol{\theta}^j) \tag{2.4}$$

where $\hat{P}_F$ is the approximation of P_F made by Monte Carlo, and it simply corresponds to the mean value of the output dataset. The accuracy in the estimation of P_F could be evaluated by the following expression:

$$\delta_{MC} = \frac{1}{\sqrt{K}} \frac{\sqrt{\frac{1}{K}\sum_{j=1}^{K} \left(I_F\left(\boldsymbol{\theta}^j\right)\right)^2 - \left(\frac{1}{K}\sum_{j=1}^{K} I_F\left(\boldsymbol{\theta}^j\right)\right)^2}}{\frac{1}{K}\sum_{j=1}^{K} I_F\left(\boldsymbol{\theta}^j\right)} \tag{2.5}$$

where δ_{MC} defines the coefficient of variation of the estimator $\hat{P}_F$. In other words, this value represents the variations obtained if the procedure to estimate $\hat{P}_F$ is repeated multiple times. Note that δ_{MC} goes to zero if K goes to infinity, indicating that the Direct Monte Carlo Method is an unbiased and convergent estimator.

Since the proposed framework requires the solution of Eq.(2.2) for any desired manufacturing tolerance δ, the computational cost could be significant. However, the Direct Monte Carlo simulation presents some advantages related to: (1) it is an unbiased and convergent method, (2) it is possible to control the precision via the number of samples, (3) the number of uncertain variables does not affect the precision and (4) imposes not constrains in the performance model complexity or in the PDF associated to the model parameters. Other techniques can be also applied to solve the probabilistic integral, e.g. asymptotic and analytical approximations. Unfortunately, these methods only provide an approximation to the probabilistic integral assuming that the integrand behaves like a Gaussian distribution. In this case, no measure of the accuracy of that approximation can be directly established. Moreover, these methods require the estimation of the integrand maximum and the evaluation of the Hessian at that point. Note that the identification of this quantities could be challenging for systems with large number of uncertainty variables.

The ultimate challenge of Monte Carlo sampling methods is to decrease the computational time required in the solution of Eq.(2.2). This issue could be tackled either by decreasing the number of samples used in the Monte Carlo simulation or by decreasing the computational time involved in the calculation of the performance metric $\mathbf{H}(\boldsymbol{\theta})$. In order to alleviate this computational burden, a computationally efficient surrogate model for $\mathbf{H}(\boldsymbol{\theta})$ was adopted. In particular, it employs a Kriging metamodel.

2.2.2 Kriging-Based Metamodel

Kriging provides a simplified relationship between the input and output of a process (for example, a computational expensive simulation model) by utilizing existing information (database) for the given process. Let assume that exist a database (training set) of n_{sup} number of $\boldsymbol{\theta} - \mathbf{H}(\boldsymbol{\theta})$ pairs (also known as support points). This training set is denoted as $\{\boldsymbol{\theta}^k - \mathbf{H}(\boldsymbol{\theta}^k) : k = 1, ..., n_{sup}\}$. Derivation of the database is formally known as DoE (Design of Experiments) and common approach is to use a space-filling algorithm for it (such as Latin Hypercube Sampling [32]) within the range Θ of possible values for $\boldsymbol{\theta}$.

The fundamental building blocks of Kriging are the n_{sup} dimensional basis vector $\mathbf{f}(\boldsymbol{\theta})$ and the correlation function $R(\boldsymbol{\theta}^n, \boldsymbol{\theta}^m)$, with typical selections corresponding, respectively, to a full quadratic basis and a generalized exponential correlation, leading to

$$\begin{aligned} \mathbf{f}(\boldsymbol{\theta}) &= \left[1 \ \theta_1 \cdots \theta_{N_\mathrm{e}} \ \theta_1^2 \ \theta_1\theta_2 \cdots \theta_{N_\mathrm{e}}^2\right] \\ \text{where } \ n_p &= (N_\mathrm{e}+1)(N_\mathrm{e}+2)/2 \\ R(\boldsymbol{\theta}^n, \boldsymbol{\theta}^m) &= \prod_{\mathrm{i}=1}^{N_\theta} exp\left[-s_\mathrm{i}|\boldsymbol{\theta}_\mathrm{i}^n - \boldsymbol{\theta}_\mathrm{i}^m|^{s_{N_\theta+1}}\right] \\ &\text{with } \ \mathbf{s} = [s_1 \cdots s_{N_\theta+1}] \end{aligned} \tag{2.6}$$

For the set of n_{sup} observations (training set) with input and their corresponding output matrix given by

$$\begin{aligned} \boldsymbol{\Phi} &= \left[\boldsymbol{\theta}^1 \cdots \boldsymbol{\theta}^{n_{sup}}\right]^T \\ \mathbf{Z} &= \left[\mathbf{H}(\boldsymbol{\theta}^1) \cdots \mathbf{H}(\boldsymbol{\theta}^{n_{sup}})\right]^T \end{aligned} \tag{2.7}$$

it is defined the basis

$$\mathbf{F} = \left[\mathbf{f}(\boldsymbol{\theta}^1) \cdots \mathbf{f}(\boldsymbol{\theta}^{n_{sup}})\right]^T \tag{2.8}$$

and the correlation matrix $\mathbf{R}$ with its nm-element defined by $R(\boldsymbol{\theta}^n, \boldsymbol{\theta}^m)$. Also for every new input $\boldsymbol{\theta}$, the correlation vector between the input and each of the elements of $\boldsymbol{\Phi}$ is defined as follow:

$$\mathbf{r}(\boldsymbol{\theta}) = \left[R(\boldsymbol{\theta}, \boldsymbol{\theta}^1) \cdots R(\boldsymbol{\theta}, \boldsymbol{\theta}^{n_{sup}})\right]^T \tag{2.9}$$

Ultimately, the Kriging approximation of the model $\mathbf{H}(\boldsymbol{\theta})$ is given by the following Gaussian process [33]:

$$\mathbf{H}(\boldsymbol{\theta}) \sim GP\left(\bar{\mathbf{H}}(\boldsymbol{\theta}), \bar{\boldsymbol{\Sigma}}(\boldsymbol{\theta})\right) \tag{2.10}$$

where $\bar{\mathbf{H}}(\boldsymbol{\theta})$ corresponds to the mean of the prediction defined as:

$$\begin{aligned} \bar{\mathbf{H}}(\boldsymbol{\theta}) &= \mathbf{f}(\boldsymbol{\theta})\boldsymbol{\alpha}^* + \mathbf{r}(\boldsymbol{\theta})^T \mathbf{R}^{-1} \left(\mathbf{Z} - \mathbf{F}\boldsymbol{\alpha}^*\right) \\ \boldsymbol{\alpha}^* &= \left(\mathbf{F}^T \mathbf{R}^{-1} \mathbf{F}\right)^{-1} \mathbf{F}^T \mathbf{R}^{-1} \mathbf{Z} \end{aligned} \tag{2.11}$$

while $\bar{\boldsymbol{\Sigma}}(\boldsymbol{\theta})$ corresponds to the covariance matrix function of the prediction defined as

$$\begin{aligned} \bar{\boldsymbol{\Sigma}}(\boldsymbol{\theta}) = \mathbf{A} \left[1 + \mathbf{u}^T \left(\mathbf{F}^T \mathbf{R}^{-1} \mathbf{F}\right)^{-1} \mathbf{u} - \mathbf{r}(\boldsymbol{\theta})^T \mathbf{R}^{-1} \mathbf{r}(\boldsymbol{\theta})\right] \\ \mathbf{u} = \mathbf{F}^T \mathbf{R}^{-1} \mathbf{r}(\boldsymbol{\theta}) - \mathbf{f}(\boldsymbol{\theta})^T \\ \mathbf{A} = \left(\mathbf{Z} - \mathbf{F}\boldsymbol{\alpha}^*\right)^T \mathbf{R}^{-1} \left(\mathbf{Z} - \mathbf{F}\boldsymbol{\alpha}^*\right) / n_{sup} \end{aligned} \tag{2.12}$$

Through the proper tuning of the parameter $\mathbf{s}$, of the correlation function, Kriging can efficiently approximate very complex functions. The tuning involves an optimization process (training process) where $\mathbf{s}$ is identified. More details on this optimization may be found

in [33]. The accuracy of the metamodel can be evaluated considering a leave-one out cross validation approach [34].

Note that $\bar{\mathbf{H}}(\boldsymbol{\theta})$ is used as the surrogate model (to estimate the exceedance probability presented in Eq.2.2) while $\bar{\boldsymbol{\Sigma}}(\boldsymbol{\theta})$ describes the variance of the process which could be used to identify the space of $\boldsymbol{\theta}$ where the trained Kriging presents important spread. The identification of this space could be exploited in order to implement an adaptive procedure in which the new support points are added only in regions where the spread are important.

Chapter 3

Global and Local Adaptive Kriging

In this chapter, the Kriging variance is used to guide an adaptive training. The general idea is to reduce the total number of support points, thus keeping the number of evaluations of the high fidelity model to a minimum. In this regard, the support points are recurrently added in order to obtain a surrogate model with a global or local precision. Both strategies are explored next.

3.1 Global Adaptive Kriging

This global strategy seeks to carry out the Kriging training (described in section 2.2.2) by adding samples exclusively in regions where the Kriging cross-validation identifies poor performance. This process is performed recursively over the entire domain of $\boldsymbol{\theta}$, leading to a global surrogate model incorporating a minimum numbers of support points. Note that this global strategy, like the standard Kriging (described in Section 2.2.2), surrogates the high fidelity model $\mathbf{H}(\boldsymbol{\theta})$ such that it could be directly used in the Monte Carlo scheme adopted to estimate the exceedance probability presented in Eq.2.2. Thus, the resulting Kriging is used to estimate the exceedance probability curve for any desired manufacturing tolerance δ, i.e., a single training is necessary.

The proposed training strategy begins employing the minimum number of support points (given by n_p in Eq.2.6) obtained using a space-filling algorithm based on the Latin Hypercube technique to generate samples of $\boldsymbol{\theta}$ and subsequently evaluate them in the high fidelity model $\mathbf{H}(\boldsymbol{\theta})$. New support points are added in an adaptive way using the cross validation of the Kriging. Cross validation is commonly applied to estimate the Kriging error and it provides a measure of its performance, which is used as a metric to identify the support points that present the most important weights in the Kriging prediction. In this particular work, this strategy aims at guiding the selection of new support points.

As is shown in [34], cross validation starts with a initial data set, consisting of n_s input-output pairs $\{\boldsymbol{\theta_s}^{\mathrm{i}} - \boldsymbol{z_s}^{\mathrm{i}}; \mathrm{i} = 1, ..., n_s\}$. First, the data is randomized and split into p mutually exclusive and exhaustive subsets, such that $\{\boldsymbol{\theta_s} - \boldsymbol{z_s}\} = \{\boldsymbol{\theta_s}^1 - \boldsymbol{z_s}^1\}, \ldots, \{\boldsymbol{\theta_s}^p - \boldsymbol{z_s}^p\}$. The metamodel is trained p times and each time leaving out one of the subsets from training and

using this omitted subset to compute the cross validation error measure. The leave-k-out approach is a variation of the p-fold cross validation. This approach considers all possible

$$\binom{n_s}{k}$$

subsets of size k are left out (where the cross validation error will be computed), and the model is trained with the remaining set. In this work, $k = 1$ is considered, which is called leave-one-out cross validation. In that way, the cross validation is computed in a loop of n_s iterations. The model is trained without the i-th element, denoted as $\boldsymbol{\theta_s}^{\sim \mathrm{i}} - \boldsymbol{z_s}^{\sim \mathrm{i}}$ and it is evaluated in this omitted point $\boldsymbol{\theta_s}^{\mathrm{i}}$ to compute the error respect to the current output $\boldsymbol{z_s}^{\mathrm{i}}$. This error is computed per support point (n_s) and output (n_z) leading to the $\mathbf{e}$ matrix. Note that large errors are associated with the support points that present important weights in the prediction. In this regard, the incorporation of new support points in their closeness decrease the cross validation error. An important issue to highlight is that each output has its own set of $\boldsymbol{\theta_s}$ that leads to large errors, i.e., same support points have different weights across the outputs. Then, different outputs could required adding new support points in different regions.

In order to facilitate the implementation of this adaptive scheme, the respective algorithm is included (Algorithm 1). The algorithm starts defining all possible values of $\boldsymbol{\theta}$ using a Latin Hypercube Sampling employing the lower possible number of samples, denoted as $\{\boldsymbol{\theta_s}^{\mathrm{i}}; \mathrm{i} = 1, ..., n_s\}$. These samples are evaluated in the high fidelity model yielding the initial training set $\{\boldsymbol{\theta_s}^{\mathrm{i}} - \boldsymbol{z_s}^{\mathrm{i}}; \mathrm{i} = 1, ..., n_s\}$. The metamodel is trained employing the available database to subsequently perform the cross validation. As discussed above, this algorithm uses the leave-one-out cross validation approach. The model is trained without the i-th element pairs $(\boldsymbol{\theta_s}^{\sim \mathrm{i}} - \boldsymbol{z_s}^{\sim \mathrm{i}})$ and it is evaluated in the omitted point $\boldsymbol{\theta_s}^{\mathrm{i}}$ yielding the predicted output of the model $\widehat{\boldsymbol{z}}^{\mathrm{i}}$. Next, the error of the model is computed as:

$$\mathbf{e} = \frac{\boldsymbol{z_s} - \widehat{\boldsymbol{z}}}{\boldsymbol{z_s}} \tag{3.1}$$

with an element-wise operation. Note that the dimension of $\mathbf{e}$ is $n_s \times n_z$. Therefore, the error is computed per support point and predicted output. This error is sorted over each system output to identify the support points with greater influence in the metamodel precision. This is accomplished with a for loop per output, which sorts the error in a descending way keeping the first a percentage (P) of errors ($\mathbf{e}^*$) and identifying their respective samples $\boldsymbol{\theta_s}^*$. The samples $\boldsymbol{\theta_s}^*$ across the outputs are stored as $\boldsymbol{\theta_s}^o$. Note that the set $\boldsymbol{\theta_s}^o$ contains the support points with major errors across the outputs, i.e., it is possible to find repeated support points in $\boldsymbol{\theta_s}^o$. Afterwards, it is computed $\boldsymbol{\theta_{cluster}}$ as the centroids of $\boldsymbol{\theta_s}^o$ using a kmeans algorithm with n_{add} clusters. If these centroids are already in the database, the algorithm converges, otherwhise these centroids are evaluated in the high fidelity model obtaining the $z(\boldsymbol{\theta_{cluster}})$. Then, the new support points are added as a union of these sets: $\boldsymbol{z_s} = [\boldsymbol{z_s}\ \boldsymbol{z_{cluster}}]$ and $\boldsymbol{\theta_s} = [\boldsymbol{\theta_s}\ \boldsymbol{\theta_{cluster}}]$. The iteration number is updated and the while loop is repeated until the stop criteria is achieved or a certain number n_{max} of cycles is obtained. Finally, the surrogate model $\boldsymbol{z_{new}}(\boldsymbol{\theta})$ is ready to be used to compute the probabilistic integral and the probability

of exceedance showed in the Eq.(2.1) and Eq.(2.2) respectively.This training can actually be used to estimate the exceedance probability for any manufacturing tolerance δ because the metamodel is trained in the whole domain of $\boldsymbol{\theta}$.

Algorithm 1 Global Adaptive Kriging

Require: $z(\theta)$: High fidelity model $\mathbb{R}^{n_\theta} \rightarrow \mathbb{R}^{n_z}$;
n_{max}: Maximum number iteration;
n_{add}: Number samples added in each step;
Ensure: $\mathbf{z_{new}}$: Kriging Training

Draw n_s samples of $\boldsymbol{\theta}$ using a Latin Hypercube algorithm, such that $\{\boldsymbol{\theta_s}^{\text{i}}; \text{i} = 1, ..., n_s\}$.
Evaluate $\boldsymbol{z}(\boldsymbol{\theta})$ in $\boldsymbol{\theta_s}$, such that $\{\boldsymbol{z_s}^{\text{i}}; \text{i} = 1, ..., n_s\}$.
Define $n = 1$;
while $n < n_{max}$ **do**
    Kriging Training with $\boldsymbol{\theta_s} - \boldsymbol{z_s} \rightarrow \boldsymbol{z_{new}}(\boldsymbol{\theta})$
    for i $\leftarrow 1$ to n_s **do** ▷ cross validation
        Kriging Training with $\boldsymbol{\theta_s}^{\sim \text{i}} - \boldsymbol{z_s}^{\sim \text{i}} \rightarrow \boldsymbol{z_{new}}(\boldsymbol{\theta})^{\text{i}}$
        Define $\widehat{\boldsymbol{z}}^{\text{i}}$ as $\boldsymbol{z_{new}}(\boldsymbol{\theta})^{\text{i}}$ evaluated at $\boldsymbol{\theta_s}^{\text{i}}$
    end for
    Define $\mathbf{e} = (\boldsymbol{z_s} - \widehat{\boldsymbol{z}})/\boldsymbol{z_s}$ (element-wise operation such that $\{\text{e}^{\text{i},j}; \text{i} = 1, ..., n_s; j = 1, ..., n_z\}$)
    Define $\boldsymbol{\theta_s}^o \leftarrow \{\}$
    for $j \leftarrow 1$ to n_z **do**
        Sort $\{\text{e}^{\text{i},j}; \text{i} = 1, ..., n_s\}$ (descending) and keep the first P errors $\rightarrow \mathbf{e^*} \in \mathbb{R}^P$
        Identify the $\boldsymbol{\theta_s}$ that corresponds to $\mathbf{e^*} \rightarrow \boldsymbol{\theta_s}^*$
        $\boldsymbol{\theta_s}^o = [\boldsymbol{\theta_s}^o \quad \boldsymbol{\theta_s}^*]$
    end for
    Define $\boldsymbol{\theta_{cluster}}$ as the centroid of $\boldsymbol{\theta_s}^o$ using a kmeans with n_{add} clusters
    if $\boldsymbol{\theta_{cluster}} \in \boldsymbol{\theta_s}$ **then**
        break
    else
        Evaluate $z(\boldsymbol{\theta_{cluster}})$, such that $\{\boldsymbol{z_{cluster}}^j; j = 1, ..., n_{\text{add}}\}$.
        Define $\boldsymbol{z_s} = [\boldsymbol{z_s} \ \boldsymbol{z_{cluster}}]$ ▷ adding new support points
        Define $\boldsymbol{\theta_s} = [\boldsymbol{\theta_s} \ \boldsymbol{\theta_{cluster}}]$ ▷ adding new support points
        $n = n + 1$
    end if
end while
return $\boldsymbol{z_{new}}(\boldsymbol{\theta})$

3.2 Local Adaptive Kriging

The global adaptive Kriging presented allows the incorporation of new support points in any region of $\boldsymbol{\theta}$, where the cross-validation error is relevant. Thus, the metamodel obtained is expected to exhibit an adequate performance in the entire domain of $\boldsymbol{\theta}$. However, the nature of the manufacturing problem studied indicates that the most important region of $\boldsymbol{\theta}$ is defined by the manufacturing tolerance (defined in the context of this work by $p(\boldsymbol{\theta})$). In this sense, a global adaptive strategy could drive new support points to regions of $\boldsymbol{\theta}$ that

are not relevant to the uncertainty propagation problem, i.e., increasing the fidelity of the surrogate model in regions where the integrand of Eq.(2.2) is negligible. In order to overcome this issue, a local scheme is presented in this section to drive the selection of new support points by exploring the Kriging's variance only in regions of $\boldsymbol{\theta}$ defined by $p(\boldsymbol{\theta})$. Hence, the metamodel obtained will present high accuracy only in regions of $\boldsymbol{\theta}$ that contain the higher uncertainties introduced by the manufacturing tolerance.

The proposed scheme starts with a Latin Hypercube sampling of $\boldsymbol{\theta}$ in the entire domain employing the lower possible number of points and subsequently introducing new support points only in region confined by $p(\boldsymbol{\theta})$. The initial Latin Hypercube sampling of $\boldsymbol{\theta}$ allows to maintain certain level of information of the high fidelity model in the entire domain of $\boldsymbol{\theta}$, while the new support points keep the total number of high fidelity model evaluations to a minimum. This characteristic of the local adaptive scheme proposed is particularly relevant for high fidelity models with high computational burden.

In contrast to the previous model, in this local scheme the manufacturing tolerance is introduced explicitly in the training process. As described previously in section 2.1, there is a relation between the distribution $p(\boldsymbol{\theta})$ and the manufacturing tolerance δ by adopting the covariance matrix of $\boldsymbol{\theta}$ as a function of δ. Following this approach, the new support points that will be added in an adaptive manner during the training will be bounded by an specific manufacturing tolerance δ.

Similar to the global adaptive scheme, the local adaptive algorithm is also presented and described in Algorithm 2. The first step of this method corresponds to the generation of samples that follow $p(\boldsymbol{\theta})$. These samples are used to perform the Monte Carlo simulations to solve Eq.(2.2). These samples are denoted as $\{\boldsymbol{\theta_o}^k; k = 1, ..., K\}$. In the second step, n_s samples in the entire domain using a Latin Hypercube algorithm are generated. Similar to the global algorithm, the initial samples n_s correspond to the minimum necessary for the Kriging training. These samples are evaluated through a high fidelity model by obtaining the support points from each output, generating a set of data denoted $\{\boldsymbol{\theta_s}^{\mathrm{i}} - \boldsymbol{z_s}^{\mathrm{i}}; \mathrm{i} = 1, ..., n_s\}$. For the base case ($n = 1$), the output model is established as $\boldsymbol{z_{new}} = \mathbf{0} \in \mathbb{R}^{K \times n_z}$ before starting the while loop. Here, the prediction from the previous iteration is saved as $\boldsymbol{z_{old}} = \boldsymbol{z_{new}}$. The model is then trained with the support points $\{\boldsymbol{\theta_s}^{\mathrm{i}} - \boldsymbol{z_s}^{\mathrm{i}}; \mathrm{i} = 1, ..., n_s\}$ and is subsequently evaluated in the samples $\{\boldsymbol{\theta_o}^k; k = 1, ..., K\}$, where the integrand of the probability integral is more relevant. In order to verify the convergence, the Hellinger distance is used as a metric between the previous and the new prediction [35].

The Hellinger distance is a metric that quantifies the discrepancy between two probability distributions and it is used in this framework as a convergence criterion. The metric is bounded in the domain [0 1], where lower values represents two similar distributions and higher values indicating greater discrepancy. The Hellinger distance is defined as:

$$D\left(p(\theta), \pi(\theta)\right) = \sqrt{\frac{1}{2} \int_{\theta} \left[\sqrt{p(\theta)} - \sqrt{\pi(\theta)}\right]^2 \mathrm{d}\theta} \tag{3.2}$$

Where $p(\theta)$ and $\pi(\theta)$ are distributions (PDF). The Hellinger distance can be also expressed

and computed as:

$$D\left(p(\theta),\pi(\theta)\right)=\sqrt{\frac{1}{2}\int_{\theta}\left[1-\sqrt{\frac{\pi(\theta)}{p(\theta)}}\right]^{2}p(\theta)\mathrm{d}\theta}\approx\sqrt{\frac{1}{2K}\sum_{\mathrm{i}=1}^{K}\left[1-\sqrt{\frac{\pi(\theta^{\mathrm{i}})}{p(\theta^{\mathrm{i}})}}\right]^{2}} \tag{3.3}$$

In order to establish a small discrepancy between the two distributions, the Hellinger distance threshold (D_t) is computed [36]. As the Hellinger distance is invariant under the coordinate transformation for $\boldsymbol{\theta}$, the Gaussian distributions were compared for simplicity. This comparison assumes the same variance (the identity covariance matrix) and difference for the mean δ_u in every dimension between two $\boldsymbol{\theta}$-dimensional multivariate Gaussian distributions. The Hellinger distance threshold is defined as:

$$D_t=\sqrt{1-\mathrm{e}^{-(n_\theta/8)(\delta_u)^2}} \tag{3.4}$$

If the Hellinger distance is lower than the threshold D_t, Algorithm 2 converges. Otherwise, the prediction errors $\mathbf{e}$ in each sample $\{\boldsymbol{\theta_o}^k; k=1,...,K\}$ is be evaluated and sorted in descending order, keeping the first P errors of $\mathbf{e}$ (the prediction error is computed employing the Kriging variance $\bar{\boldsymbol{\Sigma}}(\boldsymbol{\theta})$ in Eq.(2.12)). These higher errors are denoted as $\mathbf{e}^*$ and are used to identify the associated samples, denoted as $\boldsymbol{\theta_o}^*$. The $\boldsymbol{\theta_o}^*$ samples are located at relevant regions of $\boldsymbol{\theta}$ (from the uncertainty perspective) and are the samples that corresponds to regions where the Kriging present important variances. Subsequently, the samples $\boldsymbol{\theta_o}^*$ are clustering via kmean identifying n_{add} centroids, defined as $\boldsymbol{\theta_{cluster}}$. Then, these centroids are evaluated in the high fidelity model to obtain the $z(\boldsymbol{\theta_{cluster}})$, which are the new support points. The new support points are added to the previous support point sets such that $\boldsymbol{z_s}=[\boldsymbol{z_s}\ \boldsymbol{z_{cluster}}]$ and $\boldsymbol{\theta_s}=[\boldsymbol{\theta_s}\ \boldsymbol{\theta_{cluster}}]$. Finally, the iteration number is updated and the process is repeated until they converge or a certain number n_{max} of cycles is obtained.

Algorithm 2 Local Adaptive Kriging

Require: $p(\boldsymbol{\theta})$: PDF associated to manufacturing tolerance;
$z(\boldsymbol{\theta})$: High fidelity model $\mathbb{R}^{n_\theta} \rightarrow \mathbb{R}^{n_z}$;
n_{max}: Maximum number iteration;
n_{add}: Number samples added in each step

Ensure: $\boldsymbol{z_{new}}$: Kriging Training

Draw K samples from $p(\boldsymbol{\theta})$, such that $\{{\boldsymbol{\theta_o}}^k; k = 1, ..., K\}$.
Draw n_s samples of $\boldsymbol{\theta}$ using a Latin Hypercube algorithm, such that $\{{\boldsymbol{\theta_s}}^{\text{i}}; \text{i} = 1, ..., n_s\}$.
Evaluate $\boldsymbol{z}(\boldsymbol{\theta})$ in $\boldsymbol{\theta_s}$, such that $\{{\boldsymbol{z_s}}^{\text{i}}; \text{i} = 1, ..., n_s\}$.
Define $n = 1$;
Define $\boldsymbol{z_{new}} = \mathbf{0} \in \mathbb{R}^{K \times n_z}$
while $n < n_{max}$ **do**
    $\boldsymbol{z_{old}} = \boldsymbol{z_{new}}$;
    Kriging Training with $\boldsymbol{\theta_s} - \boldsymbol{z_s} \rightarrow \boldsymbol{z_{new}}(\boldsymbol{\theta})$
    Evaluate $\boldsymbol{z_{new}}(\boldsymbol{\theta})$ in $\boldsymbol{\theta_o}$, such that $\{{\boldsymbol{z_{new}}}^k; k = 1, ..., K\}$.
    if $D(\boldsymbol{z_{new}}, \boldsymbol{z_{old}}) < D_t$ **then** ▷ Hellinger Distance
        break
    else
        Evaluate the error of $\boldsymbol{z_{new}}(\boldsymbol{\theta})$ in $\boldsymbol{\theta_o}$, such that $\{\text{e}^k; k = 1, ..., K\}$.
        Sort $\mathbf{e}$ (descending) and keep the first P errors $\rightarrow \text{e}^*$
        Identify the $\boldsymbol{\theta_o}$ that corresponds to $\text{e}^* \rightarrow {\boldsymbol{\theta_o}}^*$
        Define $\boldsymbol{\theta_{cluster}}$ as the centroid of ${\boldsymbol{\theta_o}}^*$ using kmeans with n_{add} clusters
        Evaluate $\boldsymbol{z}(\boldsymbol{\theta_{cluster}})$, such that $\{{\boldsymbol{z_{cluster}}}^j; j = 1, ..., n_{\text{add}}\}$.
        Define $\boldsymbol{z_s} = [\boldsymbol{z_s}\ \boldsymbol{z_{cluster}}]$ ▷ adding new support points
        Define $\boldsymbol{\theta_s} = [\boldsymbol{\theta_s}\ \boldsymbol{\theta_{cluster}}]$ ▷ adding new support points
        $n = n + 1$
    end if
end while
return $\boldsymbol{z_{new}}$

Chapter 4

Effect of Uncertainties in Tilting Pad Journal Bearings

This section illustrates the implementation of the proposed adaptive schemes by evaluating the influence of manufacturing tolerances on the dynamic performance of tilting pad journal bearings (TPJP). These variable geometry hydrodynamic journal bearings are mechanical elements commonly used in high-speed turbomachinery. TPJB not only provide a low friction interface supporting the rotor weight, but represent the main source of damping in land-based turbomachinery. These mechanical elements limit rotor vibration while crossing critical speeds and enable stable operation at supercritical speeds. TPJB comprise multiple pads that are concentrically assembled within a circular shell or housing. Each pad pivots independently respect to the housing. Furthermore, the radius of curvature of the pad inner surface is different from the set bore radius of curvature. This difference, represented through a preload parameter (m in Fig.4.1), promotes the development of a convergent-divergent wedge to enhance hydrodynamic effects. The dynamic performance of these bearings is modeled through linear force coefficients. These coefficients are usually obtained by solving the Reynolds equation via finite differences method using two- or three-dimensional models. The dynamic force coefficients are a strong function of the geometric parameters of each of the pads and the bearing assembly. Small deviations from nominal values in the manufacturing of each of the pads and housing can lead to variations of the critical speed locations and stability issues [24, 25], and consequently prolonged equipment commissioning periods and costly modifications. This sensitivity and the difficulty of measuring parameters such as pad preload raise the question about the adequate selection of the manufacturing tolerance bands for these multi-component bearings.

4.1 Characteristics of the Journal Bearing Studied

The proposed local and global schemes are used to evaluate the effect of manufacturing tolerance on the dynamic performance of a tilting pad journal bearing (TPJB) previously studied in [25] and [37]. Both studies determined that small variations of the pad clearance and preload could lead to important variations in the TPJB dynamic coefficients. In particular, the referred works use a TPJB with 5 pads with a variation of 5% in the nominal clearance

and preload values. These former results required imposing specific TPJBs manufacturing tolerance values in order to obtain admissible variations in the dynamic coefficients.

Table 4.1: Tilting pad journal bearing specifications.

Number of pads	5
Configuration	Load on pad
Journal diameter	110 mm
Bearing length	44 mm
Radial bearing clearance	0.099 mm
Preload	0.264 mm
Offset	50 %
Journal speed	7300 rpm
Bearing unit load	0.4 MPa
Fluid supply temperature	40^oC
Fluid supply pressure	1.29 bar
Lubricant type	ISO VG 32

Table 4.1 lists the geometric parameters an operating conditions of the TPJB from [25] and [37]. The TPJB presented in [37] is used to illustrate the implementation of the proposed methodology. This TPJB model is used over other models without loss of generality, while there are other TPJB models [38, 39, 40] that include additional effects such as pad flexibility and deformation [41, 42, 43], the implementation of the proposed methodology is independent of the selected model and the number of parameters included. The TPJB model uses the finite element method to integrate the isothermal Reynold's equation through a perturbation approach. The procedure essentially works in two stages: first it finds the static equilibrium position (given the geometry, rotor speed, weight and fluid characteristics), followed by a perturbation analysis [44] to identify the complex dynamic stiffnesses H_{xx}, H_{xy}, H_{yx} and H_{yy} for a particular perturbation frequency, where the real part is related to the stiffness and inertia coefficients and the imaginary to the damping coefficient [23]. This model is treated as the function $\mathbf{H}(\boldsymbol{\theta})$ (in equations 2.1 and 2.2) such that:

$$\mathbf{H}(\boldsymbol{\theta}) = [H_{xx}(\boldsymbol{\theta}) \;\; H_{xy}(\boldsymbol{\theta}) \;\; H_{yx}(\boldsymbol{\theta}) \;\; H_{yy}(\boldsymbol{\theta})] \tag{4.1}$$

Figure 4.1 shows a schematic view of the TPJB under evaluation, including the definition of clearance and preload, and the nomenclature used to defined the radius and the pivot position of each pad. The effect of the manufacturing tolerance are accounted as uncertainties incorporated in the pad radius R_p and the pivot position L_p, then, $\boldsymbol{\theta}$ is defined as $\boldsymbol{\theta} = [R_{p_1} \cdots R_{p_5} \; L_{p_1} \cdots L_{p_5}]^T$. The remaining parameters presented in Table 4.1 are considered known (free of uncertainties and variations). All results presented here correspond only to synchronous perturbations, i.e. perturbation frequency coincides with rotational speed.

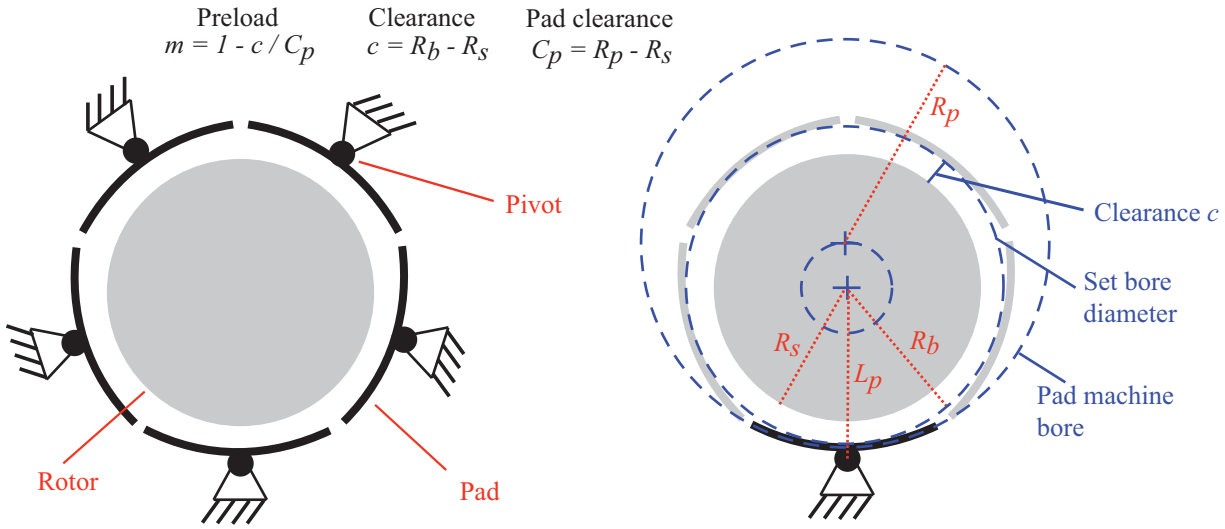

Figure 4.1: Schematic view of a 5-pad Tilting Pad Journal Bearing Describing Main Components and Geometric Parameters

The PDF $p(\boldsymbol{\theta})$ is defined as a Gaussian distribution with mean $\hat{\boldsymbol{\theta}} = [55.4 \cdots 55.4 \;\; 55.1 \cdots 55.1]^T$ (units in millimeters) while the variance of each geometrical parameter is considered as δ^2, with δ representing the manufacturing tolerance (corresponding to the case presented in Fig.2.1a). It is important to stress out that different manufacturing strategies could lead to different correlation levels between the geometrical parameters. For instance, each pad could be manufactured independently or they could be manufactured cutting in 5 parts a large pad with uniform curvature. In the former case the pad radius are uncorrelated, however, in the later manufacturing strategy, the pads will present a strong correlation. In this illustrative example, three different scenarios are evaluated: (1) a manufacturing tolerance of $10\mu m$ where all geometrical parameters are uncorrelated, (2) a manufacturing tolerance of $1\mu m$ where all geometrical parameters are uncorrelated, and (3) a manufacturing tolerance of $5\mu m$ where the pad radius are correlated in 80%.

4.2 Validation of the Proposed Adaptive Schemes

The exceedance probability curves are obtained adopting both, the local and the global adaptive schemes proposed. The validation of these schemes are achieved comparing these exceedance probability curves respect to the one obtained employing a high fidelity model, i.e., solving Eq.(2.2) without the support of any kind of metamodel. Additionally, the results are also compared with a standard Kriging to highlight the benefits of the adaptive schemes.

The comparison between the high fidelity model, the standard Kriging and the local adaptive scheme are presented in Fig.4.2. The figure shows the real and imaginary part for direct and cross-coupled dynamic stiffness coefficients, H_{xx} and H_{yx}, and for the three different tolerances described previously. Only two of the eight coefficients are presented for the sake of simplicity, however, it is possible to find the rest of coefficients in A.1. The metamodels are showed in red color (dashed lines for the standard Kriging and solid lines for the local adaptive) while the high fidelity model is presented in black solid lines. The

results show good agreements in the general trend for both metamodels. However, it is observed that the local adaptive metamodel is much closer to the high fidelity curve than the standard Kriging, where the discrepancies seems to be more important for low manufacturing tolerances and for the imaginary part of direct coefficients and the real part of cross-coupled coefficients. It is important to highlight that both metamodels are employing the same number of support points such that the differences arise exclusively from their locations.

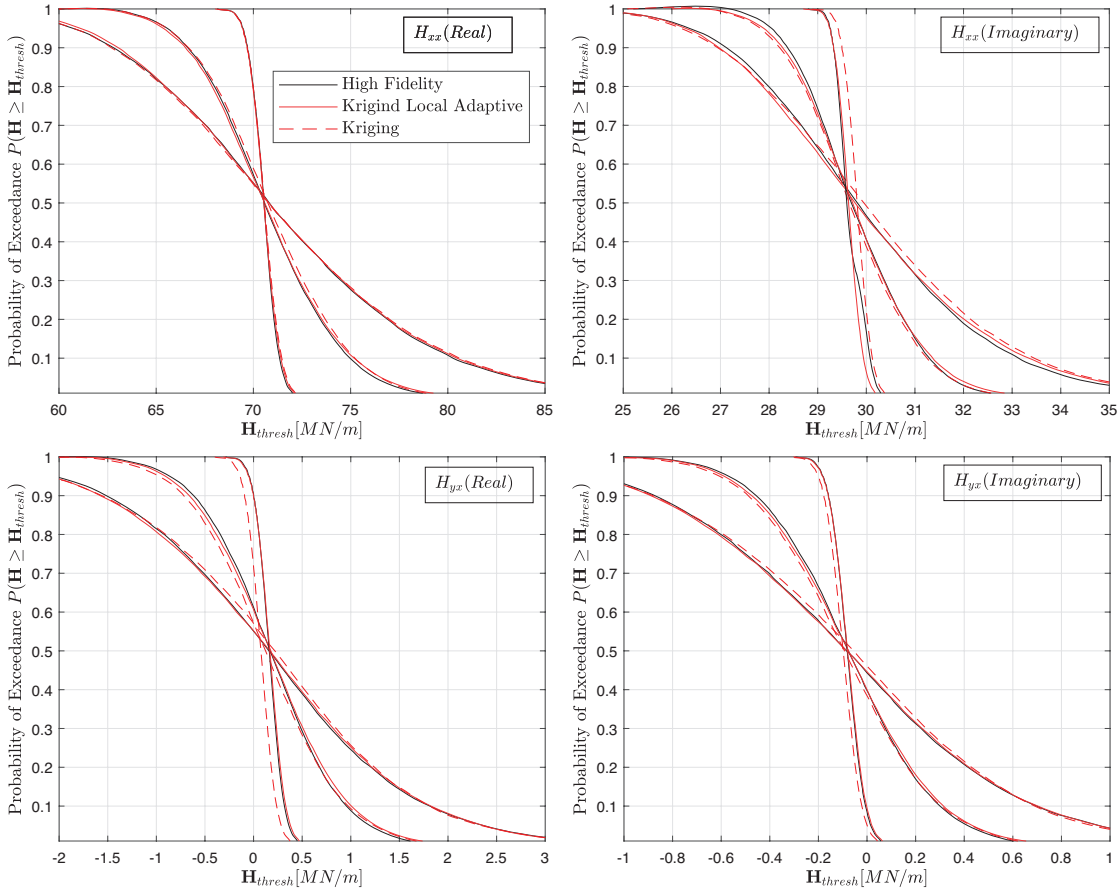

Figure 4.2: Comparison between the high fidelity model, the standard Kriging and the proposed local adaptive metamodel for H_{xx} and H_{yx} and for three different manufacturing tolerance scenarios. Important discrepancies are observed in the standard Kriging

Tables 4.2, 4.3 and 4.4 shows the local adaptive and the standard kriging prediction as percentage error respect to the high-fidelity prediction for an exceedance probability of $P_F = 0.95$ (minimum credible), $P_F = 0.5$ (median) and $P_F = 0.05$ (maximum credible). These results are presented for the uncorrelated tolerance of $10\mu m$, the uncorrelated tolerance of $1\mu m$ and the correlated tolerance of $5\mu m$, respectively (The values in $[MN/m]$ of direct and cross dynamic coefficients for the local scheme and the standard kriging can be found in A.1). Section 4.4 will explain why those values are compared.

Table 4.2: Values of direct and cross dynamic coefficient for an exceedance probability of $P_F = 0.95$ (minimum credible), $P_F = 0.5$ (median) and $P_F = 0.05$ (maximum credible) employing the high-fidelity model. The local and standard kriging prediction is presented as percentageerror respect to the high-fidelity prediction. Values corresponds to a manufacturing tolerance of $\delta = 10\mu m$ with all geometrical parameters uncorrelated.

Coef.	High Fidelity $[MN/m]$	Local Adaptive Error [%]	Standard Kriging Error [%]
	Min / Med /Max	Min / Med /Max	Min / Med /Max
$Hxx(Re)$	60.673 / 70.817 / 83.432	-0.7 / 0.0 / -0.2	-0.1 / 0.1 / -0.3
$Hyy(Re)$	23.976 / 34.724 / 53.239	0.6 / 0.3 / -0.2	0.6 / -0.4 / -0.4
$Hxy(Re)$	-2.3746 / -0.1765 / 2.0377	-2.3 / 3.6 / -0.1	-3.6 / 35.0 / 1.8
$Hyx(Re)$	-2.0394 / 0.1571 / 2.3725	-2.8 / -5.6 / -0.1	-4.2 / -39.8 / 1.8
$Hxx(Im)$	26.356 / 29.818 / 34.197	0.3 / 0.2 / -0.9	0.7 / -0.4 / -1.2
$Hyy(Im)$	14.125 / 18.325 / 25.048	0.4 / 0.1 / -0.1	0.3 / -0.3 / -0.3
$Hxy(Im)$	-0.9545 / 0.0834 / 1.1219	-0.7 / 0.2 / 1.2	-2.2 / -34.6 / 2.5
$Hyx(Im)$	-1.1159 / -0.0828 / 0.9580	-0.9 / 1.8 / 1.3	-2.2 / 34.3 / 3.2

Table 4.3: Values of direct and cross dynamic coefficient for an exceedance probability of $P_F = 0.95$ (minimum credible), $P_F = 0.5$ (median) and $P_F = 0.05$ (maximum credible) employing the high-fidelity model. The local and standard kriging prediction is presented as percentageerror respect to the high-fidelity prediction. Values corresponds to a manufacturing tolerance of $\delta = 1\mu m$ with all geometrical parameters uncorrelated.

Coef.	High Fidelity $[MN/m]$	Local Adaptive Error [%]	Standard Kriging Error [%]
	Min / Med /Max	Min / Med /Max	Min / Med /Max
$Hxx(Re)$	69.464 /70.543 / 71.593	0.0 / 0.0 / -0.1	0.0 / 0.0 / -0.2
$Hyy(Re)$	33.16 / 34.477 / 35.888	0.3 / 0.0 / -0.3	0.5 / 0.3 / 0.0
$Hxy(Re)$	-0.3787 / -0.1715 / 0.0302	-1.2 / 3.5 / -53.5	-25.3 / -50.4 / 264.5
$Hyx(Re)$	-0.0457 / 0.1613 / 0.363	-10.5 / -3.6 / -4.5	-208.7 / 53.1 / 21.8
$Hxx(Im)$	29.257 / 29.598 / 30.163	0.0 / -0.1 / 0.4	-0.5 / -0.7 / -0.2
$Hyy(Im)$	17.713 / 18.211 / 18.778	0.1 / 0.0 / 0.0	0.1 / 0.0 / 0.0
$Hxy(Im)$	-0.0161 / 0.0837 / 0.1804	-8.5 / -2.0 / -2.7	-121.7 / 20.1 / 8.2
$Hyx(Im)$	-0.1814 / -0.0815 / 0.0153	-0.9 / 2.0 / -30.1	-10.8 / -20.6 / 96.4

Looking at the first tolerance in the Table 4.2 (tolerance of $10\mu m$ with all geometrical parameters uncorrelated), it is possible to confirm what Figure 4.2 shows, the local training offers better accuracy than the standard kriging. The last one shows errors close to 40% for the cross coefficients. Then, considering a smaller manufacturing tolerance (tolerance of $1\mu m$

with all geometrical parameters uncorrelated, Table 4.3), the error increase up in the same coefficients reaching errors of up to 260% for the real part of H_{xy}.

Table 4.4: Values of direct and cross dynamic coefficient for an exceedance probability of $P_F = 0.95$ (minimum credible), $P_F = 0.5$ (median) and $P_F = 0.05$ (maximum credible) employing the high-fidelity model. The local and standard kriging prediction is presented as percentageerror respect to the high-fidelity prediction. Values corresponds to a manufacturing tolerance of $\delta = 5\mu m$ with the pad radius correlated in 80%.

Coef.	High Fidelity $[MN/m]$	Local Adaptive Error [%]	Standard Kriging Error [%]
	Min / Med /Max	Min / Med /Max	Min / Med /Max
$Hxx(Re)$	65.577 / 70.572 / 76.254	0.3 / 0.0 / -0.4	0.0 / -0.2 / -0.4
$Hyy(Re)$	28.391 / 34.491 / 42.288	0.3 / -0.3 / -0.4	1.3 / 0.8 / -0.3
$Hxy(Re)$	-1.1932 / -0.1603 / 0.8638	-3.8 / 3.3 / -7.0	-9.4 / -30.5 / -5.1
$Hyx(Re)$	-0.8618 / 0.1730 / 1.1942	-5.1 / -3.4 / -5.3	-12.9 / 28.3 / -3.9
$Hxx(Im)$	28.051 / 29.692 / 31.713	0.6 / -0.1 / -0.4	0.8 / 0.1 / 0.0
$Hyy(Im)$	15.905 / 18.227 / 21.128	0.3 / -0.2 / -0.4	0.7 / 0.3 / -0.1
$Hxy(Im)$	-0.4058 / 0.0896 / 0.5799	-3.9 / -0.1 / -3.2	-8.7 / 18.1 / -2.1
$Hyx(Im)$	-0.5701 / -0.0764 / 0.4138	-3.1 / 0.6 / -4.8	-6.5 / -20.7 / -3.6

About the third manufacturing tolerance scenario (tolerance of $5\mu m$ with the pad radious correlated in 80%, Table 4.4) the results are similar. It is possible to notice a better accuracy in the local training presenting errors up to 7% for the minimum and maximum credible value, while the standard kriging present error arround 13%. For the mean value the local scheme present errors close to 3.5% for the real part of H_{yx} while the standard kriging present errors greater than 30% for the same coefficient.

A similar comparison between the high fidelity model, the standard Kriging and the global adaptive scheme is presented in Fig.4.3. The exceedance probability curves for the same dynamic coefficients are presented. The metamodels are shown in blue (solid line for the global adaptive scheme and dashed line for the standard Kriging), while the high fidelity is presented in black solid lines as the previous figure. Similar to the previous results, the trend of the models are in agreement, however, the standard Kriging shows important discrepancies respect to the high fidelity model, specifically for the imaginary part of the direct coefficients. As in the previous case, the number of support points of the metamodels are the same and it is also possible to argue that the differences between the metamodels come exclusively from the location of the support points. Thus, the effectiveness of the adaptive scheme is proved. Please note that the number of support points employed for both adaptive schemes are not necessary the same, then, the standard Krigings in figures 4.2 and 4.3 are not directly comparable.

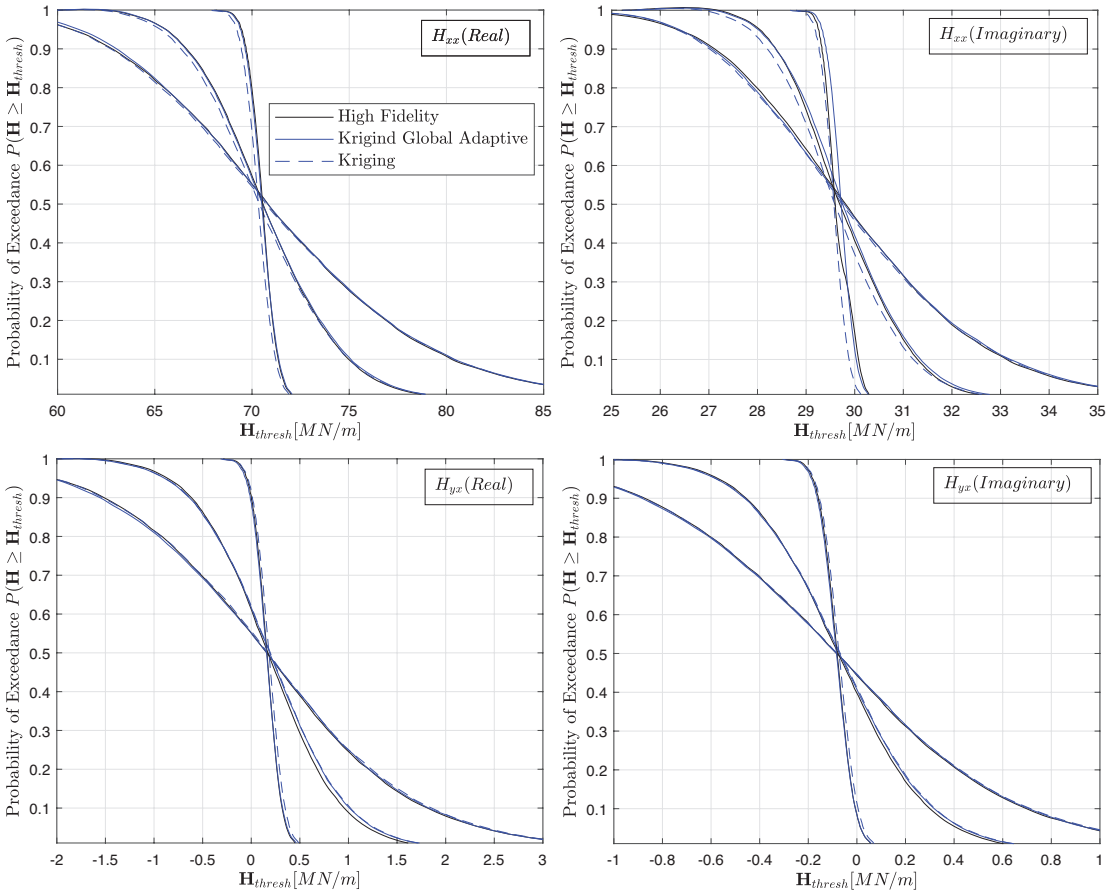

Figure 4.3: Comparison between the high fidelity model, the standard Kriging and the proposed global adaptive metamodel for H_{xx} and H_{yx} and for three different manufacturing tolerance scenarios. Important discrepancies are observed in the standard Kriging

Like in the previous analysis. Tables 4.5, 4.6 and 4.7 show the global adaptive and the standard kriging prediction as percentage error respect to the high-fidelity prediction for an exceedance probability of $P_F = 0.95$ (minimum credible), $P_F = 0.5$ (median) and $P_F = 0.05$ (maximum credible). These results are presented for the uncorrelated tolerance of $10\mu m$, the uncorrelated tolerance of $1\mu m$ and the correlated tolerance of $5\mu m$, respectively (The values in $[MN/m]$ of direct and cross dynamic coefficients for the global scheme and the standard kriging can be found in A.2).

Table 4.5: Values of direct and cross dynamic coefficient for an exceedance probability of $P_F = 0.95$ (minimum credible), $P_F = 0.5$ (median) and $P_F = 0.05$ (maximum credible) employing the high-fidelity model. The global and standard kriging prediction is presented as percentageerror respect to the high-fidelity prediction. Values corresponds to a manufacturing tolerance of $\delta = 10\mu m$ with all geometrical parameters uncorrelated.

Coef.	High Fidelity $[MN/m]$	Global Adaptive Error [%]	Standard Kriging Error [%]
	Min / Med /Max	Min / Med /Max	Min / Med /Max
$Hxx(Re)$	60.673 / 70.817 / 83.432	-0.7 / 0.0 / -0.1	0.0 / 0.2 / 0.0
$Hyy(Re)$	23.976 / 34.724 / 53.239	0.2 / 0.1 / 0.9	1.0 / -0.4 / -0.1
$Hxy(Re)$	-2.3746 / -0.1765 / 2.0377	-0.8 / 1.5 / -0.4	0.1 / 5.5 / -2.6
$Hyx(Re)$	-2.0394 / 0.1571 / 2.3725	-0.9 / -2.8 / -0.2	0.0 / -6.4 / -2.2
$Hxx(Im)$	26.356 / 29.818 / 34.197	-0.2 / 0.1 / -0.4	0.1 / 0.2 / -0.1
$Hyy(Im)$	14.125 / 18.325 / 25.048	0.3 / 0.0 / 0.7	0.3 / -0.2 / -0.2
$Hxy(Im)$	-0.9545 / 0.0834 / 1.1219	0.2 / 1.4 / -0.3	0.8 / -3.2 / -1.1
$Hyx(Im)$	-1.1159 / -0.0828 / 0.95802	-0.3 / -0.9 / -0.3	0.3 / 2.7 / -1.1

Table 4.6: Values of direct and cross dynamic coefficient for an exceedance probability of $P_F = 0.95$ (minimum credible), $P_F = 0.5$ (median) and $P_F = 0.05$ (maximum credible) employing the high-fidelity model. The global and standard kriging prediction is presented as percentageerror respect to the high-fidelity prediction. Values corresponds to a manufacturing tolerance of $\delta = 1\mu m$ with all geometrical parameters uncorrelated.

Coef.	High Fidelity $[MN/m]$	Global Adaptive Error [%]	Standard Kriging Error [%]
	Min / Med /Max	Min / Med /Max	Min / Med /Max
$Hxx(Re)$	69.464 / 70.543 / 71.593	0.1 / 0.1 / -0.1	0.4 / 0.3 / 0.2
$Hyy(Re)$	33.160 / 34.477 / 35.888	0.0 / -0.1 / -0.2	-0.5 / -0.8 / -1.0
$Hxy(Re)$	-0.3787 / -0.1715 / 0.0302	-3.7 / -2.2 / -21.0	2.1 / 12.1 / -107.1
$Hyx(Re)$	-0.0457 / 0.1613 / 0.363	-30.5 / 2.2 / -1.8	17.5 / -12.9 / -9.0
$Hxx(Im)$	29.257 / 29.598 / 30.163	-0.2 / -0.4 / 0.1	0.3 / 0.1 / 0.6
$Hyy(Im)$	17.713 / 18.211 / 18.778	-0.1 / -0.1 / 0.0	-0.4 / -0.6 / -0.5
$Hxy(Im)$	-0.0161 / 0.0837 / 0.1804	-33.6 / 3.0 / -0.3	25.5 / -9.3 / -6.6
$Hyx(Im)$	-0.1814 / -0.0815 / 0.0153	-2.9 / -2.9 / -2.1	2.2 / 9.7 / -75.7

Concerning the first tolerance set shown in the Table 4.2 (tolerance of $10\mu m$ with all geometrical parameters uncorrelated), there are not many differences between one strategy and another. Both global adaptive and standard kriging share similar errors. However, when the manufacturing tolerance is decreased to $1\mu m$, the estimation error for the minimum credible values presented by the local scheme shows errors arround the 30% only for the real

part of H_{yx} and the imaginary part of H_{xy}. On the other hand, the standard kriging presents errors arround the 20% for the same values, but the estimation error for the maximum credible values for the real part of H_{xy} and the imaginary part of H_{yx} reach errors around 107% and 75% respectively.

Table 4.7: Values of direct and cross dynamic coefficient for an exceedance probability of $P_F = 0.95$ (minimum credible), $P_F = 0.5$ (median) and $P_F = 0.05$ (maximum credible) employing the high-fidelity model. The global and standard kriging prediction is presented as percentageerror respect to the high-fidelity prediction. Values corresponds to a manufacturing tolerance of $\delta = 5\mu m$ with the pad radius correlated in 80%.

Coef.	High Fidelity $[MN/m]$	Global Adaptive Error [%]	Standard Kriging Error [%]
	Min / Med /Max	Min / Med /Max	Min / Med /Max
$Hxx(Re)$	65.577 / 70.572 / 76.254	0.0 / 0.0 / -0.3	0.4 / 0.3 / -0.1
$Hyy(Re)$	28.391 / 34.491 / 42.288	1.0 / 0.3 / -0.1	0.5 / -0.6 / -1.2
$Hxy(Re)$	-1.1932 / -0.1603 / 0.8638	-2.8 / 9.7 / -6.4	-2.6 / 14.5 / -7.9
$Hyx(Re)$	-0.8618 / 0.1730 / 1.1942	-3.6 / -8.9 / -4.9	-3.3 / -14 / -6.0
$Hxx(Im)$	28.051 / 29.692 / 31.713	0.1 / -0.2 / -0.3	0.7 / 0.3 / 0.1
$Hyy(Im)$	15.905 / 18.227 / 21.128	0.7 / 0.1 / 0.0	0.4 / -0.4 / -0.8
$Hxy(Im)$	-0.4058 / 0.0896 / 0.5799	-2.0 / -3.9 / -3.3	-2.0 / -8.8 / -4.2
$Hyx(Im)$	-0.5701 / -0.0764 / 0.4138	-1.5 / 6.0 / -4.6	-1.5 / 11.5 / -6.1

Considering the third tolerance scenario (Table 4.7) where a correlation of 80% is introduced in the pad radius, the global scheme and the standard kriging present similar results. The biggest error in the prediction is in the mean value for the same coefficient. The real part of the H_{xy} reaches values up to 9.7% and 14.5% for the global scheme and the standard kriging respectively.

Finally, both adaptive metamodels and the high fidelity models are compared for the three manufacturing tolerance and for all dynamic coefficients in Fig.4.4. An excellent agreement is observed for all cases studied.

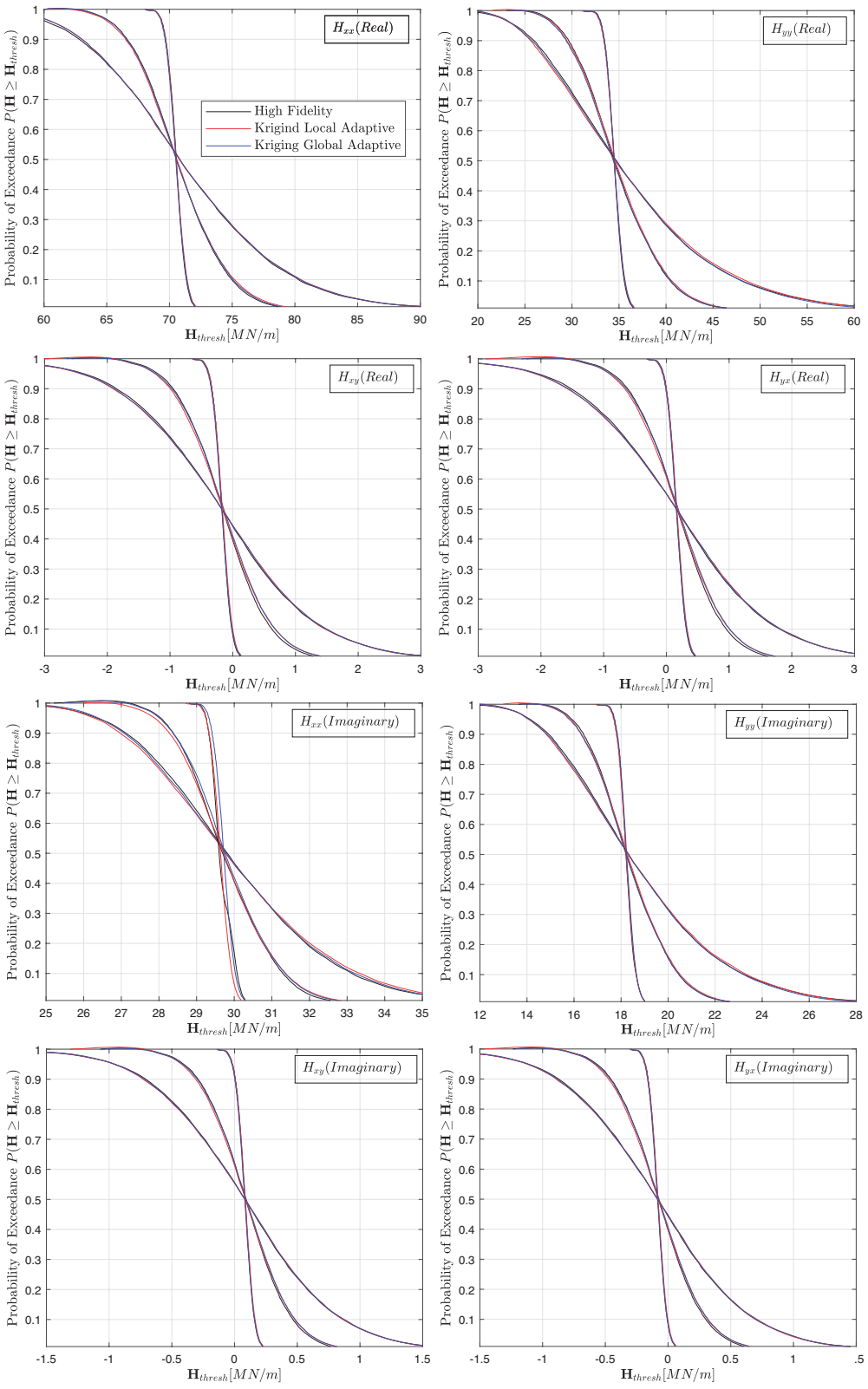

Figure 4.4: Comparison between the high fidelity model, and both adaptive metamodel proposed (local and global) for three different manufacturing tolerance scenarios. All dynamic coefficients are presented. Excellent agreement is shown for all cases

4.3 Comparison in Terms of Computational Time

Although both adaptive schemes offer similar predictions in terms of the exceedance probability, the computational time involved in each case is different. The global adaptive scheme is trained in the entire domain of $\boldsymbol{\theta}$, and thus, it is independent of the manufacturing tolerance. Thus, its training is performed once. On the other hand, the local adaptive scheme requires a training process per tolerance selected since the local training depends on the manufacturing tolerance. The high fidelity model takes more than 3hrs to obtain the exceedance probability curve for a specific tolerance, which involves 10,000 evaluations of the function $\mathbf{H}(\boldsymbol{\theta})$ used in the Monte Carlo simulation needed to solve Eq.(2.2). The computational burden offered by the proposed adaptive schemes is considerably lower than the high fidelity model, decreasing the computational burden by at least 25 times. The computational time and the fraction employed to compute each major steps in the algorithms are presented in Table 4.8. The local scheme takes almost half of the time involved in the global scheme when the first tolerance is accounted for. However,when evaluating a new tolerance condition, the global scheme is roughly 10 times faster than the local scheme. This difference is attributed to the fact that the local scheme has to perform a training process for any new tolerance set while the global scheme is already trained. In general, the local scheme seems to be a good alternative only when considering few manufacturing tolerances. The global adaptive scheme is recommended when evaluating large set of manufacturing tolerances.

Table 4.8: Computing time for the different models and tolerances

Model	High Fidelity	Local Adaptive	Global Adaptive
First Tolerance	3.23 hrs	196.14 s	407.19 s
		48% Support Points	23% Support Points
		52% Training/Prediction	75% Training
			2% Prediction
Second Tolerance	3.23 hrs	64.99 s	7.12 s
		100% Training/Prediction	100% Prediction
Third Tolerance	3.23 hrs	99.52 s	6.67 s
		100% Training/Prediction	100% Prediction

4.4 Precision for Minimum and Maximum Credible Values

The exceedance probability curves could be used to identify extreme performances. For example, to identify the minimun and maximum credible values for the dynamic coefficients of the TPJB. These credible values are defined as the dynamic coefficient that defines a probability of exceedance equal to $P_F = 0.95$ and $P_F = 0.05$ for the minimum and maximum credible values, respectively. In other words, the minimum and maximum credible values are associated with a confidence interval of 90%.

For the sake of comparison, the credible values are first obtained employing the high-fidelity model, where the accuracy of those credible values are obtained using Eq.(2.5), being $\delta_{MC} = 0.23\%$ for $P_F = 0.95$ and $\delta_{MC} = 4.36\%$ for $P_F = 0.05$. Afterwards, the credible values are obtained using the proposed adaptive schemes for the three scenarios and compared with the high-fidelity model. These results are presented in tables 4.9, 4.10 and 4.11, for the uncorrelated tolerance of $10\mu m$, the uncorrelated tolerance of $1\mu m$ and the correlated tolerance of $5\mu m$, respectively. Note that tables also presents the median dynamic coefficient ($P_F = 0.5$).

Regarding the first tolerance set (tolerance of $10\mu m$ with all geometrical parameters uncorrelated, Table 4.9), the local and global schemes offer accurate results for the minimum and maximum credible values, presenting errors up to 2.8%. However, in the median values estimation, the local scheme presents errors close to 6% for the cross coefficients while the global scheme presents errors up to 3%. When the manufacturing tolerance is decreased to $1\mu m$ (Table 4.10), the estimation error for the minimum credible values presented by the local scheme increases up to 10.5%. For this case, the maximum credible estimation values present errors greater than 5% only for the real part of H_{xy} and the imaginary part of H_{yx}, reaching errors around 54% and 30% respectively. In the global scheme, the real part of H_{yx} and the imaginary part of H_{xy} present errors around 30% in the estimation of the minimum credible value; while only the real part of H_{xy} present errors greater than 2% in the estimation for the maximum credible value. In terms of the median prediction, both adaptive schemes offer predictions with lower errors (below 4%). In general, the reduction of the manufacturing tolerance deteriorates the precision of both adaptive schemes, with a higher impact on the global scheme.

Table 4.9: Values of direct and cross dynamic coefficient for an exceedance probability of $P_F = 0.95$ (minimum credible), $P_F = 0.5$ (median) and $P_F = 0.05$ (maximum credible) employing the high-fidelity model. The local and global adaptive prediction is presented as percentage error respect to the high-fidelity prediction. Values corresponds to a manufacturing tolerance of $\delta = 10\mu m$ with all geometrical parameters uncorrelated.

Coef.	High Fidelity $[MN/m]$	Local Adaptive Error[%]	Global Adaptive Error[%]
	Min / Med /Max	Min / Med /Max	Min / Med /Max
$H_{xx}(Re)$	60.673 / 70.817 / 83.432	-0.7 / 0.0 / -0.2	-0.7 / 0.0 /-0.1
$H_{yy}(Re)$	23.976 / 34.724 / 52.239	0.6 / 0.3 / -0.2	0.2 / 0.1 / 0.9
$H_{xy}(Re)$	-2.3746 / -0.1765 / 2.0377	-2.3 / 3.6 / -0.1	-0.8 / 1.5 /-0.4
$H_{yx}(Re)$	-2.0394 / 0.1571 / 2.3725	-2.8 / -5.6 / -0.1	-0.9 / -2.8 / -0.2
$H_{xx}(Im)$	26.356 / 29.818 / 34.197	-0.3 / 0.2 / -0.9	-0.2 / 0.1 /-0.4
$H_{yy}(Im)$	14.125 / 18.325 / 25.048	0.4 / 0.1 / -0.1	0.3 / 0.0 / 0.7
$H_{xy}(Im)$	-0.9545 / 0.0834 / 1.1219	-0.7 / 0.2 / 1.2	0.2 / 1.4 /-0.3
$H_{yx}(Im)$	-1.1159 / -0.0828 / 0.9580	-0.9 / 1.8 / 1.3	-0.3 /-0.9 /-0.3

Table 4.10: Values of direct and cross dynamic coefficient for an exceedance probability of $P_F = 0.95$ (minimum credible), $P_F = 0.5$ (median) and $P_F = 0.05$ (maximum credible) employing the high-fidelity model. The local and global adaptive prediction is presented as percentage error respect to the high-fidelity prediction. Values corresponds to a manufacturing tolerance of $\delta = 1\mu m$ with all geometrical parameters uncorrelated.

Coef.	High Fidelity $[MN/m]$	Local Adaptive Error[%]	Global Adaptive Error[%]
	Min / Med /Max	Min / Med /Max	Min / Med /Max
$H_{xx}(Re)$	69.464 / 70.543 / 71.593	0.0 / 0.0 / -0.1	0.1 / 0.1 / -0.1
$H_{yy}(Re)$	33.160 / 34.477 / 35.888	0.3 / 0.0 / -0.3	0.0 / -0.1 / -0.2
$H_{xy}(Re)$	-0.3787 / -0.1715 / 0.0302	-1.2 / 3.5 / -53.5	-3.7 / -2.2 / -21.0
$H_{yx}(Re)$	-0.0457 / 0.1613 / 0.3630	-10.5 / -3.6 / -4.5	-30.5 / 2.2 / -1.8
$H_{xx}(Im)$	29.257 / 29.598 / 30.163	0.0 / -0.1 / 0.4	-0.2 / -0.4 / 0.1
$H_{yy}(Im)$	17.713 / 18.211 / 18.778	0.1 / 0.0 / 0.0	-0.1 / -0.1 / 0.0
$H_{xy}(Im)$	-0.0161 / 0.0837 / 0.1805	-8.5 / -2.0 / -2.7	-33.6 / 3.0 / -0.3
$H_{yx}(Im)$	-0.1814 / -0.0815 / 0.0154	-0.9 / 2.0 / -30.1	-2.9 / -2.9 / -2.1

Studying the third manufacturing tolerance scenario (Table 4.11) where a correlation of 80% is introduced in the pad radius, it is possible to observed that the local scheme presents a better performance when compared to the global scheme. In this case, the error identified in the local adaptive scheme reaches values up to 5% while the global adaptive scheme presents errors as high as 10%. This difference in performance is expected since the local scheme aims to increase the precision in regions of $\boldsymbol{\theta}$ where bearing geometry is more likely to lies, which is ultimately defined by $p(\boldsymbol{\theta})$.

Table 4.11: Values of direct and cross dynamic coefficient for an exceedance probability of $P_F = 0.95$ (minimum credible), $P_F = 0.5$ (median) and $P_F = 0.05$ (maximum credible) employing the high-fidelity model. The local and global adaptive prediction is presented as percentage error respect to the high-fidelity prediction. Values corresponds to a manufacturing tolerance of $\delta = 5\mu m$ with the pad radius correlated in 80%.

Coef.	High Fidelity $[MN/m]$	Local Adaptive Error[%]	Global Adaptive Error[%]
	Min / Med /Max	Min / Med /Max	Min / Med /Max
$H_{xx}(Re)$	65.577 / 70.572 / 76.254	0.3 / 0.0 / -0.4	0.0 / 0.0 / -0.3
$H_{yy}(Re)$	28.391 / 34.491 / 42.288	0.3 / -0.3 / -0.4	1.0 / 0.3 / -0.1
$H_{xy}(Re)$	-1.1932 / -0.1603 / 0.8638	-3.8 / 3.3 / -7.0	-2.8 / 9.7 / -6.4
$H_{yx}(Re)$	-0.8618 / 0.1730 / 1.1942	-5.1 / -3.4 / -5.3	-3.6 / -8.9 / -4.9
$H_{xx}(Im)$	28.051 / 29.692 / 31.713	0.6 / -0.1 / -0.4	0.1 / -0.2 / -0.3
$H_{yy}(Im)$	15.905 / 18.227 / 21.128	0.3 / -0.2 / -0.4	0.7 / 0.1 / 0.0
$H_{xy}(Im)$	-0.4058 / 0.0896 / 0.5799	-3.9 / -0.1 / -3.2	-2.0 / -3.9 / -3.3
$H_{yx}(Im)$	-0.5701 / -0.0764 / 0.4138	-3.1 / 0.6 / -4.8	-1.5 / 6.0 / -4.6

Chapter 5

Conclusions

A robust framework to identify the relationship between the manufacturing tolerance of a mechanical part and the expected variations on its mechanical performance is presented. The framework is based on a Monte Carlo simulation adopting a surrogate model in order to predict the probability to exceed a certain performance. The surrogate model, based on Kriging interpolation, is trained in an adaptive way with the use of a deterministic model. Two different approaches to train the model are presented: local and global. Both adaptive schemes offer a reduction in the computing time and similar predictions in terms of exceedance probability of mechanical performance. These methods were compared with a traditional Kriging employing the same number of support points showing a better accuracy in the adaptives schemes, where the only differences were from the location of them. As far as the author's knowledge, the use of this kind of procedures in the selection of manufacturing tolerance by means of adaptive Kriging metamodels was not fully studied until now.

A study of the reliability of a tilting pad journal bearing was presented employing the proposed framework. The implementation of this technique is not straightforward since it requires a certain expertise, which is the reason why it was decided to revisit the most important concepts and adapt them to the study of TPJB. As result, the use of metamodels in the study of the reliability of a TPJB demonstrated a series of significant advantages as: (1) it is possible to evaluate the influence of manufacturing tolerances on the dynamic performance (2) the most probable value of the dynamic coefficients are identified, (3) it is possible to identify the minimum and maximum credible values for its dynamic coefficients, and (4) the exceedance probability curves could be used to identify extreme performances. The methodology is validated comparing these exceedance probability curves respect to the one obtained employing a high fidelity model. Although this research focused on a particular bearing configuration, the framework is extendable to any other mechanical component. In general, the proposed framework represents a feasible and attractive approach to define manufacturing tolerance limits with minimum computational effort.

Finally, considering the versatility of this methodology, the implementation of this scheme to any other mechanical component is proposed for future work. Also, it could be interesting to develop a sensitivity analysis to implement on this scheme. This type of analysis would allows the identification of the parameter or set of parameters that have the greatest influence

on the model output. It consequently provides useful insight into which model input contributes most to the variability of the model output. In this particular case, the dimensions that have the greatest influence on the performance would be identified, thus strict tolerance specifications on them would be applied.

Bibliography

[1] A. Standard, "Dimensioning and tolerancing, asme y14. 5m-1994," *American Society of Mechanical Engineers, New York*, 1994.

[2] I. G. P. Specifications, "Geometrical tolerancing—tolerances of form, orientation, location and run-out. iso 1101: 2004," *International Standard Organization, Geneva*, 2005.

[3] E. Morse, J. Y. Dantan, N. Anwer, R. Söderberg, G. Moroni, A. Qureshi, X. Jiang, and L. Mathieu, "Tolerancing: Managing uncertainty from conceptual design to final product," *CIRP Annals*, vol. 67, no. 2, pp. 695–717, 2018.

[4] S. Gupta and J. U. Turner, "Variational Solid Modeling," *IEEE Computer Graphics and Applications*, pp. 64–74, 1993.

[5] N. Anwer, A. Ballu, and L. Mathieu, "The skin model, a comprehensive geometric model for engineering design," *CIRP Annals - Manufacturing Technology*, vol. 62, no. 1, pp. 143–146, 2013.

[6] N. Anwer, B. Schleich, L. Mathieu, and S. Wartzack, "From solid modelling to skin model shapes: Shifting paradigms in computer-aided tolerancing," *CIRP Annals - Manufacturing Technology*, vol. 63, no. 1, pp. 137–140, 2014.

[7] B. Schleich, N. Anwer, L. Mathieu, and S. Wartzack, "Skin model shapes: A new paradigm shift for geometric variations modelling in mechanical engineering," *Computer-Aided Design*, vol. 50, pp. 1–15, 2014.

[8] B. Schleich and S. Wartzack, "Approaches for the assembly simulation of skin model shapes," *Computer-Aided Design*, vol. 65, pp. 18–33, 2015.

[9] J. Liu, Z. Zhang, X. Ding, and N. Shao, "Integrating form errors and local surface deformations into tolerance analysis based on skin model shapes and a boundary element method," *Computer-Aided Design*, vol. 104, pp. 45–59, 2018.

[10] W. Huang and D. Ceglarek, "Mode-based Decomposition of Part Form Error by Discrete-Cosine-Transform with Implementation to Assembly and Stamping System with Compliant Parts," *CIRP Annals*, vol. 51, no. 1, pp. 21–26, 2002.

[11] S. Samper, J.-P. Petit, and M. Giordano, "Computer Aided Tolerancing - Solver and Post Processor Analysis," *Advances in Design*, pp. 487–497, 2006.

[12] M. Giordano, S. Samper, and J. P. Petit, "Tolerance analysis and synthesis by means of deviation domains, axi-symmetric cases," *Models for Computer Aided Tolerancing in Design and Manufacturing - Selected Conference Papers from the 9th CIRP International Seminar on Computer-Aided Tolerancing, CAT 2005*, pp. 85–94, 2007.

[13] J. K. Davidson, A. Mujezinovi, and J. J. Shah, "A new mathematical model for geometric tolerances as applied to round faces," *Journal of Mechanical Design, Transactions of the ASME*, vol. 124, no. 4, pp. 609–622, 2002.

[14] A. Mujezinovi, J. K. Davidson, and J. J. Shah, "A new mathematical model for geometric tolerances as applied to polygonal faces," *Journal of Mechanical Design, Transactions of the ASME*, vol. 126, no. 3, pp. 504–518, 2004.

[15] K. Jiang, J. K. Davidson, J. Liu, and J. J. Shah, "Using tolerance maps to validate machining tolerances for transfer of cylindrical datum in manufacturing process," *International Journal of Advanced Manufacturing Technology*, vol. 73, no. 1-4, pp. 465–478, 2014.

[16] G. Ameta, S. Serge, and M. Giordano, "Comparison of Spatial Math Models for Tolerance Analysis: Tolerance-Maps, Deviation Domain, and TTRS," *Journal of Computing and Information Science in Engineering*, vol. 11, no. 2, p. 021004, 2011.

[17] H. Chen, S. Jin, Z. Li, and X. Lai, "A comprehensive study of three dimensional tolerance analysis methods," *Computer-Aided Design*, vol. 53, pp. 1–13, 2014.

[18] M. Hallmann, S. Goetz, and B. Schleich, "Mapping of gd&t information and pmi between 3d product models in the step and stl format," *Computer-Aided Design*, vol. 115, pp. 293–306, 2019.

[19] B. Louhichi, M. Tlija, A. Benamara, and A. Tahan, "An algorithm for cad tolerancing integration: generation of assembly configurations according to dimensional and geometrical tolerances," *Computer-Aided Design*, vol. 62, pp. 259–274, 2015.

[20] A. Armillotta, "A method for computer-aided specification of geometric tolerances," *Computer-Aided Design*, vol. 45, no. 12, pp. 1604–1616, 2013.

[21] R. Askri, C. Bois, H. Wargnier, and N. Gayton, "Tolerance synthesis of fastened metal-composite joints based on probabilistic and worst-case approaches," *Computer-Aided Design*, vol. 100, pp. 39–51, 2018.

[22] A. J. Qureshi, J.-Y. Dantan, V. Sabri, P. Beaucaire, and N. Gayton, "A statistical tolerance analysis approach for over-constrained mechanism based on optimization and monte carlo simulation," *Computer-Aided Design*, vol. 44, no. 2, pp. 132–142, 2012.

[23] D. Child, *Turbomachinery rotordynamics: phenomena, modeling, and analysis*. 1993.

[24] W. Dmochowski, A. Dadouche, and M. Fillon, "Numerical study of the sensitivity of tilting-pad journal bearing performance characteristics to manufacturing tolerances: Dynamic analysis," *Tribology Transactions*, vol. 51, no. 5, pp. 573–580, 2008.

[25] J. C. Romero Quintini, S. Pineda, J. A. Matute, L. U. Medina, J. L. Gómez, and S. E. Diaz, "Determining the effect of bearing clearance and preload uncertainties on tilting pad bearings rotordynamic coefficients," in *Turbo Expo: Power for Land, Sea, and Air*, vol. 45776, p. V07BT32A021, American Society of Mechanical Engineers, 2014.

[26] K. Feng, M. Shi, T. Gong, Y. Liu, and J. Zhu, "A novel squeeze-film air bearing with flexure pivot-tilting pads: Numerical analysis and measurement," *International Journal of Mechanical Sciences*, vol. 134, pp. 41–50, 2017.

[27] C. B. Khatri and S. C. Sharma, "Analysis of textured multi-lobe non-recessed hybrid journal bearings with various restrictors," *International Journal of Mechanical Sciences*, vol. 145, pp. 258–286, 2018.

[28] P. Novotnỳ and J. Hrabovskỳ, "Efficient computational modelling of low loaded bearings of turbocharger rotors," *International Journal of Mechanical Sciences*, vol. 174, p. 105505, 2020.

[29] K. Maharshi, T. Mukhopadhyay, B. Roy, L. Roy, and S. Dey, "Stochastic dynamic behaviour of hydrodynamic journal bearings including the effect of surface roughness," *International Journal of Mechanical Sciences*, vol. 142, pp. 370–383, 2018.

[30] C. E. Merelli, D. O. Barilá, G. G. Vignolo, and L. M. Quinzani, "Dynamic coefficients of finite length journal bearing. evaluation using a regular perturbation method," *International Journal of Mechanical Sciences*, vol. 151, pp. 251–262, 2019.

[31] R. Rosenkrantz, *E. T. Jaynes: Papers on Probability, Statistics and Statistical Physics*. 1983.

[32] M. D. McKay, R. J. Beckman, and W. J. Conover, "A comparison of three methods for selecting values of input variables in the analysis of output from a computer code," *Technometrics*, vol. 21, no. 2, pp. 239–245, 1979.

[33] S. N. Lophaven, H. B. Nielsen, J. Sondergaard, and A. Dace, "A matlab kriging toolbox," *Technical University of Denmark, Kongens Lyngby, Technical Report No. IMMTR-2002*, vol. 12, 2002.

[34] M. Meckesheimer, R. R. Barton, T. W. Simpson, and A. J. Booker, "Computationally inexpensive metamodel assessment strategies," *Proceedings of the ASME Design Engineering Technical Conference*, vol. 2, no. 10, pp. 191–201, 2001.

[35] J. Zhang and A. A. Taflanidis, "Adaptive Kriging Stochastic Sampling and Density Approximation and Its Application to Rare-Event Estimation," *ASCE-ASME Journal of Risk and Uncertainty in Engineering Systems, Part A: Civil Engineering*, vol. 4, no. 3, 2018.

[36] G. Jia and A. A. Taflanidis, "Sample-based evaluation of global probabilistic sensitivity measures," *Computers and Structures*, vol. 144, pp. 103–118, 2014.

[37] J. L. Gomez, S. Pineda, and S. E. Diaz, "On the effect of pad clearance and preload

manufacturing tolerances on tilting pad bearings rotordynamic coefficients," in *Turbo Expo: Power for Land, Sea, and Air*, vol. 55270, p. V07BT30A022, American Society of Mechanical Engineers, 2013.

[38] L. San Andrés and Y. Tao, "The role of pivot stiffness on the dynamic force coefficients of tilting pad journal bearings," in *Turbo Expo: Power for Land, Sea, and Air*, vol. 55270, p. V07BT30A013, American Society of Mechanical Engineers, 2013.

[39] T. Dimond, A. A. Younan, P. Allaire, and J. Nicholas, "Modal frequency response of a four-pad tilting pad bearing with spherical pivots, finite pivot stiffness, and different pad preloads," *Journal of Vibration and Acoustics*, vol. 135, no. 4, 2013.

[40] J. Yang and A. Palazzolo, "Three-dimensional thermo-elasto-hydrodynamic computational fluid dynamics model of a tilting pad journal bearing—part ii: Dynamic response," *Journal of Tribology*, vol. 141, no. 6, 2019.

[41] A. Delgado, G. Vannini, B. Ertas, M. Drexel, and L. Naldi, "Identification and prediction of force coefficients in a five-pad and four-pad tilting pad bearing for load-on-pad and load-between-pad configurations," *Journal of engineering for gas turbines and power*, vol. 133, no. 9, 2011.

[42] J. C. Wilkes and D. W. Childs, "Tilting pad journal bearings—a discussion on stability calculation, frequency dependence, and pad and pivot," *Journal of engineering for gas turbines and power*, vol. 134, no. 12, 2012.

[43] J. E. Gaines and D. W. Childs, "The impact of pad flexibility on the rotordynamic coefficients of tilting-pad journal bearings," *Journal of Engineering for Gas Turbines and Power*, vol. 138, no. 8, 2016.

[44] J. W. Lund, "Spring and Damper Coefficients for the Tilting-Pad Journal Bearing," *Tribology Transactions*, vol. 7, no. 4, pp. 342–352, 1964.

Annex A

Values of Direct and Cross Dynamic Coefficient

A.1 Local Adaptive Kriging and Standard Kriging

Tables A.1, A.2 and A.3 show the values of direct and cross dynamic coefficient for an exceedance probability of $P_F = 0.95$ (minimum credible), $P_F = 0.5$ (median) and $P_F = 0.05$ (maximum credible) employing the high-fidelity model, the local adaptive training and the standard kriging.

Table A.1: Values of direct and cross dynamic coefficient for an exceedance probability of $P_F = 0.95$ (minimum credible), $P_F = 0.5$ (median) and $P_F = 0.05$ (maximum credible) employing the high-fidelity model, local adaptive prediction and standard kriging. Values corresponds to a manufacturing tolerance of $\delta = 10\mu m$ with all geometrical parameters uncorrelated.

Coef.	High Fidelity $[MN/m]$	Local Adaptive $[MN/m]$	Standard Kriging $[MN/m]$
	Min / Med /Max	Min / Med /Max	Min / Med /Max
$Hxx(Re)$	60.673 / 70.817 / 83.432	61.084 / 70.800 / 83.609	60.723 / 70.778 / 83.683
$Hyy(Re)$	23.976 / 34.724 / 53.239	23.822 / 34.604 / 53.348	23.827 / 34.851 / 53.475
$Hxy(Re)$	-2.3746 / -0.1765 / 2.0377	-2.429 / -0.1701 / 2.0398	-2.4594 / -0.1147 / 2.0018
$Hyx(Re)$	-2.0394 / 0.1571 / 2.3725	-2.0963 / 0.1660 / 2.3753	-2.1243 / 0.2197 / 2.3306
$Hxx(Im)$	26.356 / 29.818 / 34.197	26.276 / 29.769 / 34.510	26.176 / 29.949 / 34.609
$Hyy(Im)$	14.125 / 18.325 / 25.048	14.069 / 18.297 / 25.067	14.082 / 18.380 / 25.114
$Hxy(Im)$	-0.9545 / 0.0834 / 1.1219	-0.9610 / 0.0833 / 1.1085	-0.9758 / 0.1123 / 1.0939
$Hyx(Im)$	-1.1159 / -0.0828 / 0.9580	-1.126 / -0.0813 / 0.9455	-1.1401 / -0.0544 / 0.9278

Table A.2: Values of direct and cross dynamic coefficient for an exceedance probability of $P_F = 0.95$ (minimum credible), $P_F = 0.5$ (median) and $P_F = 0.05$ (maximum credible) employing the high-fidelity model, local adaptive prediction and standard kriging. Values corresponds to a manufacturing tolerance of $\delta = 1\mu m$ with all geometrical parameters uncorrelated.

Coef.	High Fidelity $[MN/m]$	Local Adaptive $[MN/m]$	Standard Kriging $[MN/m]$
	Min / Med /Max	Min / Med /Max	Min / Med /Max
$Hxx(\mathrm{Re})$	69.464 / 70.543 / 71.593	69.442 / 70.535 / 71.662	69.445 /70.565 / 71.721
$Hyy(\mathrm{Re})$	33.160 / 34.477 / 35.888	33.075 / 34.484 / 35.985	32.979 / 34.387 / 35.892
$Hxy(\mathrm{Re})$	-0.3787 / -0.1715 / 0.0302	-0.3834 / -0.1655 / 0.0464	-0.4745 / -0.2579 / -0.0497
$Hyx(\mathrm{Re})$	-0.0457 / 0.1613 / 0.3630	-0.0504 / 0.1672 / 0.3793	-0.1411 / 0.0756 / 0.2840
$Hxx(Im)$	29.257 / 29.598 / 30.163	29.248 / 29.634 / 30.030	29.415 / 29.810 / 30.216
$Hyy(Im)$	17.713 / 18.211 / 18.778	17.688 / 18.213 / 18.776	17.687 / 18.212 / 18.774
$Hxy(Im)$	-0.0161 / 0.0837 / 0.1804	-0.0175 / 0.0853 / 0.1854	-0.0357 / 0.0669 / 0.1657
$Hyx(Im)$	-0.1814 / -0.0815 / 0.0153	-0.1831 / -0.0799 / 0.0200	-0.2010 / -0.0983 / 0.00054

Table A.3: Values of direct and cross dynamic coefficient for an exceedance probability of $P_F = 0.95$ (minimum credible), $P_F = 0.5$ (median) and $P_F = 0.05$ (maximum credible) employing the high-fidelity model, local adaptive prediction and standard kriging. Values corresponds to a manufacturing tolerance of $\delta = 5\mu m$ with the pad radius correlated in 80%.

Coef.	High Fidelity $[MN/m]$	Local Adaptive $[MN/m]$	Standard Kriging $[MN/m]$
	Min / Med /Max	Min / Med /Max	Min / Med /Max
$Hxx(\mathrm{Re})$	65.577 / 70.572 / 76.254	65.375 / 70.584 / 76.578	65.561 / 70.748 / 76.541
$Hyy(\mathrm{Re})$	28.391 / 34.491 / 42.288	28.305 / 34.580 / 42.471	28.032 / 34.220 / 42.426
$Hxy(\mathrm{Re})$	-1.1932 / -0.1603 / 0.8638	-1.2382 / -0.155 / 0.9239	-1.3054 / -0.2092 / 0.9077
$Hyx(\mathrm{Re})$	-0.8618 / 0.1730 / 1.1942	-0.9055 / 0.1788 / 1.257	-0.9727 / 0.1241 / 1.2412
$Hxx(Im)$	28.051 / 29.692 / 31.713	27.890 / 29.717 / 31.844	27.820 / 29.647 / 31.716
$Hyy(Im)$	15.905 / 18.227 / 21.128	15.863 / 18.271 / 21.205	15.787 / 18.164 / 21.159
$Hxy(Im)$	-0.4058 / 0.0896 / 0.5799	-0.4218 / 0.0897 / 0.5986	-0.4410 / 0.0734 / 0.5922
$Hyx(Im)$	-0.5701 / -0.0764 / 0.4138	-0.5876 / -0.0759 / 0.4335	-0.6074 / -0.0922 / 0.4287

Figure A.1 shows the probability of exceedance for all dynamic coefficients for the three different tolerances employing the high-fidelity model, local adaptive prediction and standard kriging.

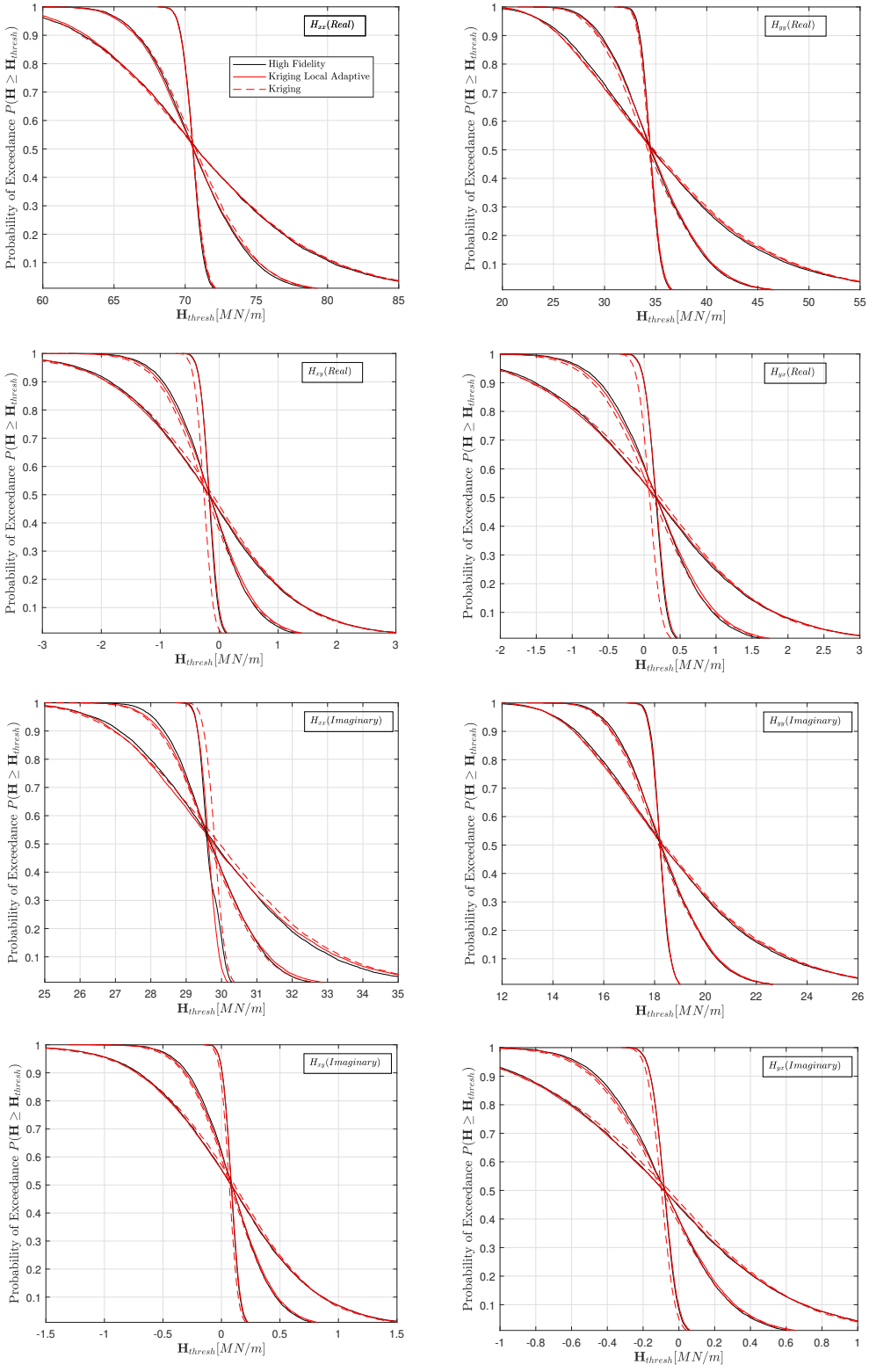

Figure A.1: Comparison between the high fidelity model, the standard Kriging and the proposed local adaptive metamodel for the dynamic coefficients for three different manufacturing tolerance scenarios. Important discrepancies are observed in the standard Kriging

A.2 Global Adaptive Kriging and Standard Kriging

Tables A.4, A.5 and A.6 show the values of direct and cross dynamic coefficient for an exceedance probability of $P_F = 0.95$ (minimum credible), $P_F = 0.5$ (median) and $P_F = 0.05$ (maximum credible) employing the high-fidelity model, the global adaptive training and the standard kriging.

Table A.4: Values of direct and cross dynamic coefficient for an exceedance probability of $P_F = 0.95$ (minimum credible), $P_F = 0.5$ (median) and $P_F = 0.05$ (maximum credible) employing the high-fidelity model, global adaptive prediction and standard kriging. Values corresponds to a manufacturing tolerance of $\delta = 10\mu m$ with all geometrical parameters uncorrelated.

Coef.	High Fidelity $[MN/m]$	Global Adaptive $[MN/m]$	Standard Kriging $[MN/m]$
	Min / Med /Max	Min / Med /Max	Min / Med /Max
$Hxx(Re)$	60.673 / 70.817 / 83.432	61.080 / 70.805 / 83.548	60.703 / 70.710 / 83.453
$Hyy(Re)$	23.976 / 34.724 / 53.239	23.923 / 34.699 / 52.769	23.748 / 34.876 / 53.315
$Hxy(Re)$	-2.3746 / -0.1765 / 2.0377	-2.3939 / -0.1739 / 2.0453	-2.3713 / -0.1667 / 2.0907
$Hyx(Re)$	-2.0394 / 0.1571 / 2.3725	-2.0587 / 0.1616 / 2.3772	-2.040 / 0.1672 / 2.4243
$Hxx(Im)$	26.356 / 29.818 / 34.197	26.397 / 29.783 / 34.321	26.342 / 29.748 / 34.229
$Hyy(Im)$	14.125 / 18.325 / 25.048	14.088 / 18.328 / 24.873	14.079 / 18.370 / 25.091
$Hxy(Im)$	-0.9545 / 0.0834 / 1.1219	-0.9530 / 0.0823 / 1.1252	-0.9473 / 0.0861 / 1.1338
$Hyx(Im)$	-1.1159 / -0.0828 / 0.9580	-1.1191 / -0.0835 / 0.9613	-1.1123 / -0.0806 / 0.9686

Table A.5: Values of direct and cross dynamic coefficient for an exceedance probability of $P_F = 0.95$ (minimum credible), $P_F = 0.5$ (median) and $P_F = 0.05$ (maximum credible) employing the high-fidelity model, global adaptive prediction and standard kriging. Values corresponds to a manufacturing tolerance of $\delta = 1\mu m$ with all geometrical parameters uncorrelated.

Coef.	High Fidelity $[MN/m]$	Global Adaptive $[MN/m]$	Standard Kriging $[MN/m]$
	Min / Med /Max	Min / Med /Max	Min / Med /Max
$Hxx(Re)$	69.464 / 70.543 / 71.593	69.408 / 70.505 / 71.633	69.203 / 70.326 / 71.477
$Hyy(Re)$	33.160 / 34.477 / 35.888	33.146 / 34.507 / 35.959	33.338 / 34.743 / 36.237
$Hxy(Re)$	-0.3787 / -0.1715 / 0.0302	-0.3927 / -0.1753 / 0.0366	-0.3706 / -0.1508 / 0.0626
$Hyx(Re)$	-0.0457 / 0.1613 / 0.363	-0.0596 / 0.1577 / 0.3694	-0.0376 / 0.1822 / 0.3957
$Hxx(Im)$	29.257 / 29.598 / 30.163	29.329 / 29.720 / 30.121	29.182 / 29.573 / 29.975
$Hyy(Im)$	17.713 / 18.211 / 18.778	17.723 / 18.237 / 18.782	17.787 / 18.313 / 18.871
$Hxy(Im)$	-0.0161 / 0.0837 / 0.1804	-0.0215 / 0.0812 / 0.1809	-0.0120 / 0.0915 / 0.1923
$Hyx(Im)$	-0.1814 / -0.0815 / 0.0153	-0.1867 / -0.0839 / 0.0156	-0.1773 / -0.0736 / 0.0270

Table A.6: Values of direct and cross dynamic coefficient for an exceedance probability of $P_F = 0.95$ (minimum credible), $P_F = 0.5$ (median) and $P_F = 0.05$ (maximum credible) employing the high-fidelity model, global adaptive prediction and standard kriging. Values corresponds to a manufacturing tolerance of $\delta = 5\mu m$ with the pad radius correlated in 80%.

Coef.	High Fidelity $[MN/m]$	Global Adaptive $[MN/m]$	Standard Kriging $[MN/m]$
	Min / Med /Max	Min / Med /Max	Min / Med /Max
$Hxx(\mathrm{Re})$	65.577 / 70.572 / 76.254	65.555 / 70.545 / 76.457	65.291 / 70.392 / 76.322
$Hyy(\mathrm{Re})$	28.391 / 34.491 / 42.288	28.100 / 34.400 / 42.316	28.238 / 34.713 / 42.799
$Hxy(\mathrm{Re})$	-1.1932 / -0.1603 / 0.8638	-1.2263 / -0.1448 / 0.9195	-1.2247 / -0.1371 / 0.9323
$Hyx(\mathrm{Re})$	-0.8618 / 0.1730 / 1.1942	-0.8927 / 0.1884 / 1.2529	-0.8902 / 0.1972 / 1.2663
$Hxx(Im)$	28.051 / 29.692 / 31.713	28.017 / 29.753 / 31.815	27.850 / 29.593 / 31.685
$Hyy(Im)$	15.905 / 18.227 / 21.128	15.795 / 18.212 / 21.130	15.846 / 18.307 / 21.294
$Hxy(Im)$	-0.4058 / 0.0896 / 0.5799	-0.4137 / 0.0931 / 0.5988	-0.4139 / 0.0975 / 0.6040
$Hyx(Im)$	-0.5701 / -0.0764 / 0.4138	-0.5785 / -0.0718 / 0.4327	-0.5785 / -0.0675 / 0.4391

Figure A.2 shows the probability of exceedance for all dynamic coefficients for the three different tolerances employing the high-fidelity model, global adaptive prediction and standard kriging.

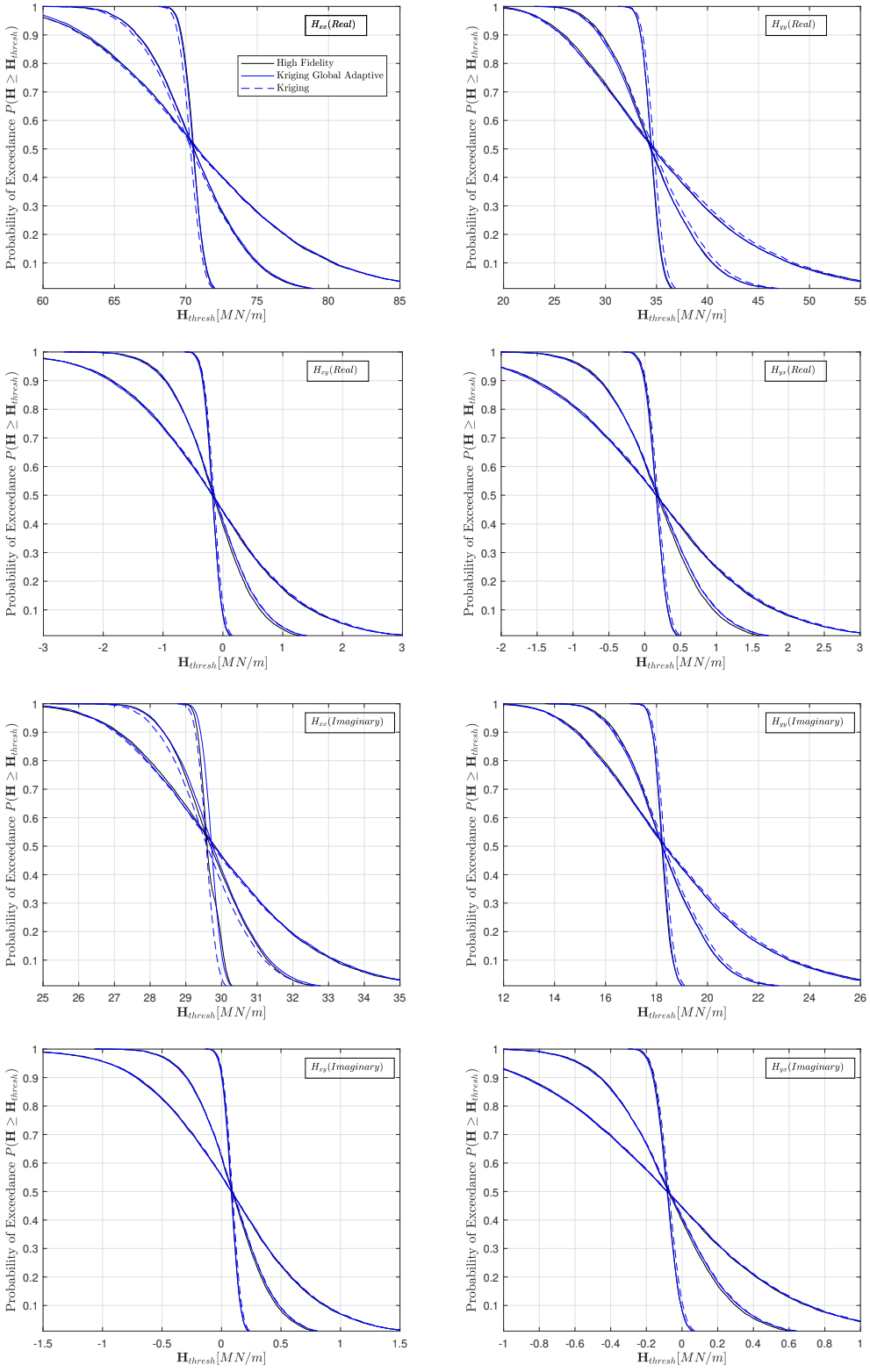

Figure A.2: Comparison between the high fidelity model, the standard Kriging and the proposed global adaptive metamodel for the dynamic coefficients for three different manufacturing tolerance scenarios. Important discrepancies are observed in the standard Kriging